THE ASTROPHYSICAL JOURNAL, 362:74–89, 1990 October 10

BOWEN FLUORESCENCE IN A SAMPLE OF SEYFERT NUCLEI[1]

JONATHAN SCHACHTER,[2] ALEXEI V. FILIPPENKO,[3,4] AND STEVEN M. KAHN[2,3,5]
University of California, Berkeley
Received 24 August 1989; accepted 1990 April 11

ABSTRACT

We discuss new observations of the O III and N III Bowen fluorescence lines in a sample of two Seyfert 2 nuclei and six Seyfert 1 nuclei with relatively narrow permitted lines. Included are new measurements of O III $\lambda\lambda$3133, 3444, which are the two strongest cascades produced in the Bowen process, and possible detections of O III λ3341, a secondary cascade expected to be produced following emission of a λ3133 photon. Our data cover a wide spectral range, from the atmospheric limit at $\sim$3100 Å out to redward of [S II] $\lambda\lambda$6716, 6731. Measurements of the [S II] and [O III] lines are used to estimate densities for the program objects.

Using the flux-calibrated spectra and the Bowen yields, together with the derived electron densities, we construct a model spherical Bowen-emitting region. This region, which has a derived radius of 1–10 pc, has a small filling factor (10^{-7} to 10^{-3}). The clouds cover the central source, but are optically thin to the soft X-ray continuum emitted at the source. Many ($\sim 10^{10}$) clouds, of size $\sim$1–1000 AU, inhabit the emitting region. The total required mass in clouds is $\sim$100–10^6 $M_\odot$.

Subject headings: atomic processes — galaxies: nuclei — galaxies: Seyfert — line formation

I. INTRODUCTION

In a previous paper (Schachter, Filippenko, and Kahn 1989, hereafter Paper I), we analyzed Bowen fluorescence (BF) in the Scorpius X-1 binary system. We confirmed the existence of BF in this source by measuring O III $\lambda\lambda$3133, 3444—the strongest expected Bowen emission lines (Saraph and Seaton 1980). The O III lines, which arise in an emission-line region (ELR) ionized by X-rays produced near the neutron star, are cascades produced when He II Lyα (λ303.783) pumps the $2p3d$ level of O III (Bowen 1934). Since the relevant pumping transitions are optically thick ($\tau > 10^4$ typically), He II Lyα undergoes multiple scatterings. The principal fates of He II Lyα photons are (1) escape from the BF line region, (2) photoionization of H I or He I, or (3) conversion to a Bowen line. We refer to the fraction of He II Lyα converted to O III Bowen lines as *the helium-oxygen Bowen yield* ($y_{\rm HeO}$).

Observational constraints on $y_{\rm HeO}$ may be derived from line ratios of the form $I_{\rm O\,III}/I_{\rm He\,II}$, where $I_{\rm O\,III}$ is the intensity of any strong Bowen line (usually λ3133 or λ3444) and $I_{\rm He\,II}$ is the intensity of any He II recombination line (usually λ4686 [Paα] or λ3204 [Paβ]). Strengths of oxygen Bowen lines relative to λ3133 have been calculated, as have strengths of He II lines relative to λ4686. Because of the lack of detectors sensitive shortward of 3400 Å in the past, $y_{\rm HeO}$ was first defined in terms of I_{3444}/I_{4686} (Harrington 1972). In compact X-ray sources, the observed value of I_{3444}/I_{4686} can be large, leading to estimates of $y_{\rm HeO} \gtrsim 0.3$. Analysis of the Bowen process (Kallman and McCray 1980, hereafter KM80) shows that $y_{\rm HeO}$ should be a sensitive function of the He II Lyα optical depth, $\tau_{\rm L}$, and hence that measurements of $I_{\rm O\,III}/I_{\rm He\,II}$ can be used to derive limits on $\tau_{\rm L}$. In addition, the He II emission measure (EM) can be inferred from $I_{\rm He\,II}$. For Sco X-1, we used the observationally derived constraints on EM and $\tau_{\rm L}$ to set reasonable limits on the size and density of an assumed spherical Bowen ELR. We found evidence that BF arises in the low-density outer fringe of a denser structure, confined within the Roche lobe of the primary. Thus, we were able to show that measurements of BF *in and of themselves* could be used to give important information on the structure of the ELR in Sco X-1.

The techniques developed in Paper I are versatile enough that they may be extended to ELRs of many other accretion-powered sources. In the current work, we consider BF in a carefully selected sample of active galaxies—Seyfert 2 nuclei and narrow-line Seyfert 1 nuclei. In these sources, BF can be used to set independent constraints on the structure of the narrow-line region (NLR).

O III Bowen lines have previously been detected in only a small number of Seyfert nuclei because of the difficulties of observing near the atmospheric limit. Osterbrock (1981) reported $\lambda\lambda$3133, 3444 (the latter blended with [Ne V] λ3426) in the high-ionization Seyfert 1 galaxy III Zw 77. Shuder and Osterbrock (1981) found these oxygen lines in the Seyfert 2 galaxies Akn 347 and I Zw 92, but the use of a small rectangular aperture could have led to inaccurate UV flux calibration, due to atmospheric dispersion. They also reported λ3444 in the type 2 Seyferts UM 16 and Mrk 622, although the data on these two galaxies cannot be used to calculate $y_{\rm HeO}$. In particular, for UM 16, λ3444 is contaminated by incomplete removal of Hg I λ3651 (a night-sky line from mercury lamps), while for Mrk 622, λ3444 lies too close to the blue end of the scan for accurate fluxing (Eastman and MacAlpine 1985). Eastman and MacAlpine found λ3444 in Mrk 573 (= UM 363; Seyfert 2). In the first extensive study of BF in active galactic nuclei (AGNs), Malkan (1986) obtained flux-calibrated spectra of 9 Seyfert 1 and Seyfert 2 nuclei with measurable λ3133. The Seyfert 1s and high-excitation Seyfert 2s have significantly larger (typically by a factor of 2) values of I_{3133}/I_{4686} than the low-excitation Seyfert 2s. We note that N III Bowen lines have been undetected in Seyferts, the single exception being the possible detection in NGC 3783 (Stirpe, de Bruyn, and van Groningen 1988; Seyfert 1).

[1] Based on observations made at Lick Observatory, which is owned and operated by the University of California.
[2] Department of Physics and Space Sciences Laboratory.
[3] Department of Astronomy.
[4] Presidential Young Investigator.
[5] Also affiliated with Laboratory for Experimental Astrophysics at Lawrence Livermore National Laboratory.

Since BF is a resonant process involving He II, O III, and in some cases N III, a clear proof of its existence demands (1) detection of as many fluorescent lines as possible (e.g., $\lambda\lambda$3133 *and* 3444 whenever available), with line ratios in accord with those expected from atomic physics calculations, and (2) simultaneous detection of emission lines that give the pumping line strength (e.g., He II λ3204), with reasonable values of Bowen yields. Without these checks, the single reports of Bowen lines are dubious. Our analysis requires an unambiguous detection in a flux-calibrated spectrum.

Given these observational requirements, we have conducted a careful study of Bowen emission in Seyfert 2 and narrow-line Seyfert 1 nuclei, using a Cassegrain CCD spectrograph on the 3 m Shane reflector at Lick Observatory. Strong $\lambda\lambda$3133, 3204 are seen in all objects reported here. In addition, some show $\lambda\lambda$3341, 3444 and N III BF, and our high-resolution work is useful in deblending lines (where necessary). More than half of the objects in our Seyfert sample have never been observed below [Ne V] λ3346. For the first time, we present complete, flux-calibrated spectra from the atmospheric limit at $\sim$3100 Å to wavelengths as red as [S II] $\lambda\lambda$6716, 6731. These new observations give additional diagnostics useful for determining temperatures, densities, and metallicities. The central goal of this work is to use the Bowen observations to characterize the line-emitting gas in Seyfert NLRs.

We begin by describing the sample of Seyfert nuclei together with special observing techniques (§ II). An improved method for the removal of atmospheric ozone bands is also discussed. Next, we give a thorough treatment of the Bowen and related line emission in each object, together with derived reddening values and density diagnostics (§ III). After determining the Bowen yields for individual sources, we use photoionization models to derive constraints on NLR structure (§ IV). We summarize our results in § V.

II. OBSERVATIONAL PROGRAM

All measurements were made with the blue-sensitive UV Schmidt system (Miller and Stone 1987) at the Cassegrain focus of the 3 m Shane reflector at Lick Observatory. Below, we briefly discuss the observational sample and the techniques used to acquire and reduce the data.

a) The Sample

Given the methods and equipment used (§ II*b*), we chose Seyfert nuclei that generally had characteristics favorable for detecting Bowen emission. The emphasis of our study was not to evaluate the prevalence of the Bowen process in Seyfert galaxies, but merely to investigate the implications of the Bowen emission lines for cases in which they can be detected. We selected galaxies with $z \geq 0.01$, so that λ3133 was redshifted to a region of the spectrum less severely affected by ozone absorption bands. Because differential slit losses caused by atmsopheric dispersion are a serious problem in near-UV observations, we confined ourselves to objects with relatively high declination ($\delta_{1950} > 4°$, except for Mrk 1126, where $\delta \approx -15°$). Also, we chose relatively bright objects ($14 \leq V \leq 17$) in order to do multiple observations at a range of grating settings for each Seyfert, while completing the study in a reasonable length of time ($\sim$2 yr).

Since many known Seyfert nuclei fall within these general criteria (e.g., see Table 3 of Véron-Cetty and Véron 1987), we narrowed the sample by inspecting previously published spectra and tables of line fluxes for $\lambda \gtrsim 3400$ Å (Cohen 1983; Davidson and Kinman 1978; Koski 1978; Osterbrock 1985; Osterbrock and Pogge 1985; Shuder and Osterbrock 1981). Two of the chosen objects are type 2 Seyferts, whose lines are narrow. The type 1 Seyferts in the sample lack strong Fe II emission lines, which would make it difficult to measure accurate strengths of the Bowen lines and He II $\lambda\lambda$3204, 4686 (Netzer and Wills 1983; Phillips 1978). In addition, they are narrow-line Seyfert 1s (Osterbrock and Pogge 1985), typically with FWHM = 700–1000 km s^{-1} for the broad components. These characteristics allow us to detect, or deblend from adjacent lines, λ3444 in some objects. They also ensure that λ4686 is not severely contaminated by the blue wing of Hβ. One final criterion is that the chosen Seyferts possess unusually high ionization, often with strong [Fe VII] and [Fe X]. Owing to the high ionization, He II λ4686 is prominent.

Table 1 lists the sample of Seyfert nuclei in order of increasing right ascension, giving Seyfert type, redshift, and *V*-magnitude (for the entire galaxy rather than only for the nucleus). For comparison purposes, we included in the sample some of the objects with previous reports of Bowen emission (§ I); these are noted in column (5) of the table. Column (6) lists references to individual spectra and tables of line fluxes.

b) Observing Techniques

As detailed in Paper I, observations in the near-UV must take account of differential slit losses due to atmospheric dispersion, as well as ozone absorption bands (in the range $\sim$3100–3400 Å). Both of these effects demanded that we perform all near-UV observations as close to the meridian as possible. We carefully placed the slit (of width 3.″2) along the parallactic angle corresponding to the midpoint of observations to avoid differential slit losses (Filippenko 1982). To remove the ozone bands, we divided the near-UV spectrum of each object by a scaled absorption template—the spectrum of an intrinsically featureless star. We describe an improvement in the ozone division over that used in Paper I later in this section.

Spectra were extracted from the two-dimensional CCD data at the grating settings specified in Table 1 of Paper I (*UV*, *blue*, *green*, *orange*, *red*, and *IR*). We synthesized a 3.″2 × 3.″3 effective aperture by summing the central five CCD pixels (0.″67 pixel^{-1}) in each case. The approximately square shape was chosen so that different grating settings sampled nearly the same portion of the NLR, despite the changing slit position angles. While it sacrificed some spectral resolution, the 3.″2 slit

TABLE 1

SAMPLE OF BOWEN SEYFERT NUCLEI

Name (1)	Type[a] (2)	z[a] (3)	V[a] (4)	Previous Bowen (5)	Spectra Reference (6)
UM 16	2	0.058	17	λ3133	1
Mrk 975	1	0.050	14.95	...	2
Mrk 359	1	0.017	14.22	...	3
MCG 8-11-11	1	0.020	14.62	...	2
Akn 347	2	0.022	14.44	λ3133	4
Mrk 1388	1	0.021	16	...	5
III Zw 77	1	0.034	15.2	$\lambda\lambda$3133, 3444	6, 7
Mrk 1126	1	0.010	14.33	...	8

[a] Values from Véron-Cetty and Véron 1987. *V* units are magnitudes.

REFERENCES.—(1) Malkan 1986; (2) Cohen 1983; (3) Davidson and Kinman 1978; (4) Shuder and Osterbrock 1981; (5) Osterbrock 1985; (6) Osterbrock 1981; (7) Ferland and Osterbrock 1987; (8) Osterbrock and Pogge 1985.

TABLE 2

OBSERVATION LOG

Date (UT)	Object	Exposure Time (hr)	Approximate Seeing (arcsec)	Air Mass
1986 Dec 1	MCG 8-11-11	2.0	1.5–2	1.0–1.1
	Mrk 359	1.7	1.5	1.1–1.4
	UM 16	2.8	1.0–1.5	1.2–1.5
1987 May 22	Akn 347	2.1	1.0	1.1–1.4
1987 May 23	Akn 347	0.75	1.5	1.1
	III Zw 77	2.8	1.0–1.5	1.0–1.2
1987 May 24	Akn 347	1.5	1.5–2	1.1
	III Zw 77	1.3	1.5–2.0	1.0
1987 Nov 22	MCG 8-11-11	1.1	2.0	1.1–1.2
1987 Nov 23	MCG 8-11-11	0.67	1.5	1.2–1.4
	Mrk 359	1.9	1.5–2.0	1.0–1.5
	UM 16	2.8	1.5–2.0	1.2–1.3
1988 Jan 14	Akn 347	1.6	2.0	1.1
	MCG 8-11-11	1.1	1.5–2.0	1.0
	Mrk 359	1.8	2.0–2.5	1.2–1.4
	UM 16	0.83	1.5	1.6–2.0
1988 Jul 16	Mrk 1388	2.0	2.0–2.5	1.1–1.8
1988 Jul 17	Mrk 1388	1.2	1.5–2.5	1.2–1.4
1988 Jul 18	Mrk 1388	0.69	2.0–2.5	1.7–2.3
	III Zw 77	0.36	1.5–2.0	1.3–1.4
1988 Sep 14	Mrk 975	1.0	1.0–1.5	1.3
	Mrk 1126	0.75	1.0–1.5	1.6
1988 Sep 15	Mrk 359	0.17	1.5	1.1
	Mrk 975	1.2	1.5	1.2–1.3
	Mrk 1126	4.6	1.5–2.0	1.7–2.4
	UM 16	0.33	1.5	1.4

width was less affected by poor or variable seeing than a narrower slit. As a check on the absolute λ4686 flux, we also obtained wide (8″) slit spectra at the green setting (~4400–5200 Å) for most objects. In some objects, the NLR is quite spatially extended, and this measurement was substantially higher than the small-aperture flux, but in any case it gave a firm upper limit to the total λ4686 flux in the nucleus. To verify the continuity of the spectrum from setting to setting, we obtained lower resolution spectra of some objects over the entire UV-IR spectral range (with a 3″.2 slit) at two new settings: *optical* (300 groove mm^{-1} grating blazed at 4200 Å; range 3100–6300 Å; no filter) and *IR2* (300 groove mm^{-1} grating blazed at 7500 Å; range 6000–9200 Å; GG 495 filter). Spectra were taken on 12 nights, over a period of almost 2 yr. Table 2 gives a journal of observations, including total exposure times, approximate seeing, and air mass. Generally, multiple observations of a single object were used to build up signal in the faint lines and to check consistency.

As described in Paper I, we had previously removed ozone absorption bands by division by an absorption template made up of two standard star spectra (sdO + sdFG). In the current data set, we obtained better results by using as a template a hot DA white dwarf, which should have no intrinsic absorption lines from the atmospheric limit to the Balmer limit. To demonstrate the effectiveness of the DA technique, we used the spectrum of one DA (EG 139; air mass 1.4) to remove the ozone from the spectrum of another DA (EG 162; air mass 1.8). In Figure 1 we present spectra before and after division, which show that the technique works well (cf. Paper I, Fig. 2). We first started taking DA spectra on 1988 July 16. On subsequent observing nights, we generally took spectra of two different DA stars, to remove ozone in Seyferts observed at low and high air masses. Approximate removal of absorption bands from pre-1988 July Seyfert spectra was accomplished by using a DA spectrum obtained at a later date, taking care to shift wavelength scales appropriately (by comparison of arc lines) before performing the division. Note that most of the Seyferts were available for study at low air mass, where ozone absorption is minimal. In forthcoming papers we apply this ozone removal technique to new near-UV spectra of X-ray binaries and

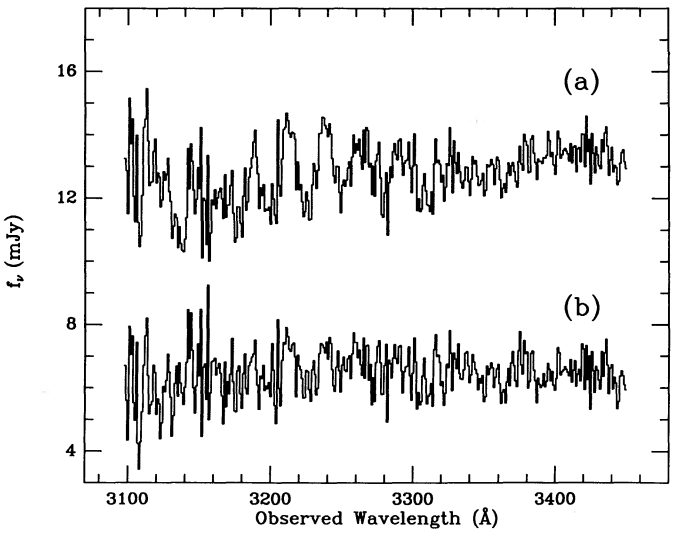

FIG. 1.—Demonstration of our technique of removing atmospheric ozone absorption bands. Near-UV spectra of the DA white dwarf EG 162, (*a*) before and (*b*) after removal of ozone, are shown. In (*b*), the prominent absorption bands are almost absent.

cataclysmic variables. For the Galactic objects, the effectively zero redshift and (in many cases) high air mass combine to make ozone absorption a much greater problem.

In general, we reduced the two-dimensional data using the basic techniques described in Paper I. However, special care needed to be taken with Seyfert nuclei, because starlight from the host galaxy can contaminate the observed spectrum, especially at wavelengths longer than the Balmer limit. For example, the Ca II H and K stellar absorption lines are evident in some of our CCD spectra. Since nonstellar light from the active nucleus dominates the central pixels, with the fractional stellar contribution increasing radially outward, we extracted the 3".2 slit spectra from a narrow (3".3) swath on the CCD. We also extracted $\sim 5''$ and $\sim 7''$ swaths for comparison, to confirm that small undulations in the continuum (caused by focus variations) were being adequately removed during the subsequent processing of the one-dimensional spectra. The wide-slit (8") spectra were extracted with a 10" swath, to get the total λ4686 flux. Note that $y_{\rm HeO}$, which depends only on I_{3133}/I_{3204} (§ IV), is essentially unaffected by stellar absorption at the moderate resolution of our spectra.

We assembled the complete spectrum from the individual, high-dispersion segments. As a check on the continuum shape, we compared different spectra of the same object, and also used spectra from the optical and IR2 settings when available (Mrk 1388 and III Zw 77 only). From the lines in the overlap region, we discovered that the derived wavelengths agreed poorly (within 1–4 Å) because of a grating tilt controller problem (see Paper I). We therefore used the night-sky lines as a guide to correct the observed wavelengths. Since the correction implied by the sky lines was not always consistent with the apparent shift in our spectra, we estimate that the wavelengths of observed lines are accurate to within $\sim$0.5–1 Å overall.

Assembling the spectrum provides a way to verify the flux calibration (continuum slope and level) in the regions of overlap. In some cases, the agreement from setting to setting was good (5%–10%) and the spectrum could be pieced together by simply averaging the regions of overlap. However, in other cases the agreement was poor ($\sim$50%). The inconsistency may be attributed to seeing variations and nonphotometric conditions, since the intrinsic continuum in the sample objects has previously been found not to vary over time scales comparable to our typical exposure times, $\sim$1–4 hr (Table 2). Narrow-line fluxes have not been observed to vary on time scales less than several months (Peterson 1988).

We expect that the flux inferred from our 3".2 × 3".3 extractions will be reliable if most of the light of a given object is concentrated in the central few pixels of the two-dimensional CCD detector. We verified the flux calibration of each program object in one or more of the following ways:

1. Comparison of green spectra from 3".2 × 5" and 3".2 × 7" extractions with the (canonical) 3".2 × 3".3 extraction. For a standard star taken with good seeing and approximately photometric conditions, the wider extractions contain 10%–20% more flux than the narrowest extraction. This is equally true for the program objects which appear almost stellar (e.g., UM 16). Other objects (e.g., Mrk 1126) are more extended, having significantly more light ($\sim$50%) in both lines and continuum in the wide extractions. This suggests the presence of an extended NLR.

2. Analysis of the image profile from the two-dimensional CCD detector. We compared the green profiles of each program object against that night's standard stars, to distinguish the effects of seeing from those of extended emission regions.

3. Comparison of green 8" and 3".2 slits. Most sample objects were observed with both a wide 8" slit and a 3".2 slit at the green setting. Since some of the program objects appear to have extended narrow-line gas, we do not expect agreement between the 8" and 3".2 derived fluxes. We find at worst a difference of a factor of 2. The discrepancy in most cases can be explained by the smaller area of the canonical extraction.

4. Comparison of spectra taken on different nights. In general, spectra of a single object taken on different nights were consistent, differing only by a scale factor (typically $\sim$1–2) which presumably represents the changes in atmospheric transparency and seeing.

Because of the many comparison tests and consistency checks we have performed, our techniques produce properly fluxed spectra that have the spectral resolution required for a thorough analysis. We are confident that the quoted fluxes are generally accurate to $\sim$20%, more than sufficient for the rough estimate of Bowen ELR structure which we discuss in § IV.

III. NEW RESULTS

In this section we briefly discuss the Bowen and related line emission of each object in our study. The spectra are displayed in Figures 2 and 3, and the relevant line intensities are listed in Table 3. We also use our observations to derive values of the reddening, and n_e constraints from observed [S II] and [O III] line intensity ratios.

a) Overview of Spectra

For each of the sample objects we have summed together different sets of observations to produce a single overall spectrum. No correction for starlight has been applied, since starlight makes a small contribution to the overall spectrum in the region occupied by the Bowen lines.

We focus now on the observations relevant to the Bowen process; these include the near-UV spectrum and the possibility of N III Bowen emission in the green region. A Grotrian diagram giving the important O III Bowen cascade wavelengths and predicted line strengths (taken from Saraph and Seaton 1980; hereafter SS) is provided in Figure 4. All the objects in our study show O III λ3133 and He II λ3204 emission, thus facilitating the calculation of Bowen yields (§ IV*a*). Other strong cascades (O III $\lambda\lambda$3341, 3429, 3444) may be present, often blended with [Ne V] λ3346 or λ3426. Below we comment specifically on objects which show additional evidence of Bowen emission.

i) *UM 16*

The 3133 and 3204 Å lines are strong (Fig. 2*a*). We find good agreement ($\sim$12%) between our value of I_{3133}/I_{3204} and that of Malkan (1986). We would also expect λ3444 to be strong, since the Bowen branching ratios imply $I_{3444}/I_{3133} = 0.28$ (Fig. 4). If λ3444 is present, it may be part of a blend centered on 3447 Å. We find $I_{\rm blend}/I_{3133} = 0.35$ after dereddening (see § III*b*). Unfortunately, the resolution is not sufficiently high to allow deblending of λ3444. In Table 3 we give the full blend intensity as an upper limit to I_{3444}. O III λ3341 is the strongest predicted cascade following the emission of λ3133, with $I_{3341}/I_{3133} = 0.14$ (Fig. 4). The 3341 Å line may be blended with [Ne V] λ3346, since I_{3426}/I_{3346} is less than the theoretical value of 2.7 (Osterbrock 1989), where I_{3426} is the intensity of [Ne V] λ3426. Also, O III λ3429 may be blended with λ3426,

TABLE 3

EMISSION-LINE INTENSITIES[a]

Ion	λ (Å)	UM 16	Mrk 975	Mrk 359	MCG 8-11-11	Akn 347	Mrk 1388	III Zw 77	Mrk 1126
O III	3133	0.35	0.94	1.04	1.56	0.16	0.47	0.82	0.21
He II	3204	0.22	0.76	0.27	0.71	0.14	0.25	0.37	0.22
O III	3299	...	...	...	...	...	0.10	...	...
O III	3312	...	...	...	...	...	0.08	...	...
O III	3341	0.06	...	0.22	...	...	<0.36	0.20	...
[Ne V]	3346	0.58	1.26	0.93	1.10	...	0.88	0.87	0.61
[Ne V]	3426	1.46	4.70	2.14	2.75	...	1.47[c]	1.87[c]	1.95
O III	3444	<0.13	...	0.15	0.67	...	0.15	0.20	0.07
N III	4640	...	...	<0.28	...	...	...	...	...
He II	4686	0.62	...	0.87	1.21:	0.34	0.65	0.73[c]	0.59
Hβ	4861	1.71	...	1.93[c]	6.70[c]	0.89	1.40[c]	1.06[c]	0.99:[c]
...	3300[b]	0.13	0.97	0.98	1.75	0.13	0.10	0.49	0.53

NOTE.—A colon indicates that flux is approximate; deblending of broad and narrow components is difficult.

[a] Observed fluxes. Not dereddened. Units are 10^{-14} ergs cm^{-2} s^{-1}.

[b] Continuum flux in mJy.

[c] Profile has broad and narrow components; quoted flux is for narrow component only.

although the Bowen cascade would be quite faint in comparison with the [Ne V] line ($\sim 0.02\, I_{3426}$ in this object). The λ3346 profile cannot be deblended, but we may estimate

$$I_{3341} \approx I^{*}_{3346} - \frac{(I^{*}_{3426} - 0.09 I_{3133})}{2.7}, \qquad (1a)$$

where the asterisks indicate blended intensities, i.e.,

$$I^{*}_{3426} = I_{[\mathrm{Ne\ V}]\lambda 3426} + I_{\mathrm{O\ III}\ \lambda 3429}, \qquad (1a)$$

$$I^{*}_{3346} = I_{[\mathrm{Ne\ V}]\lambda 3346} + I_{\mathrm{O\ III}\ \lambda 3341}. \qquad (1b)$$

Our approach gives a value of I_{3341}/I_{3133} (=0.17) which agrees reasonably well with the predicted value. We use the correct dereddened line intensities to determine I_{3341}/I_{3133}. However, for consistency with the other observed line fluxes listed in Table 3, we quote the *reddened* value of I_{3341}.

Despite the abundant evidence for oxygen Bowen lines, UM 16 appears to lack the N III Bowen lines (Fig. 3*a*).

ii) *Mrk 975*

The spectra of this object were obtained near the end of our study, so the spectral coverage through the narrow slit (observed wavelength ~ 3100–4600 Å) is limited compared with that of the other program galaxies (§ II*b*). We have included it in our discussion, however, because its spectrum exhibits some new properties not found in the other galaxies.

The λ3133 profile (Fig. 2*b*) is broad; we estimate that the line has FWHM ≈ 2000 km s^{-1}. [Ne V] λ3346 has an asymmetric profile, which might indicate the presence of O III λ3341 (see above discussion of UM 16). However, in this object [Ne V] λ3426 has a peculiar, broad red wing centered at ~3440 Å. We find (Table 3) that the residual blend intensity is $I^{\mathrm{blend}}_{3426} - 2.7 I_{3346} \approx 1.4\, I_{3133}$ ($\approx 0.28\, I^{\mathrm{blend}}_{3426}$). From Figure 4, we might expect a contribution to the residual blend intensity from O III λλ3429, 3444, but the predicted intensity is only $0.37 I_{3133}$; thus, the blends cannot be understood in a simple manner. Note that the derived blend intensity is really a lower limit, since λ3346 may be blended with λ3341.

A second possibility involves the O3 process. As described in Paper I, Deguchi (1985) has suggested that in X-ray binaries He II Lyα can be converted into O III λ303.783 (O3), with subsequent cascade lines at 3432, 3407, 3416 Å. All of these lines could be part of the 3426 Å blend. The precise value of these cascades relative to λ3133 (an O1 cascade) depends on the details of the He II Lyα (hereafter Lyα) profile, since typically O3 lies far in the wing of Lyα (KM80). However, we may obtain an upper limit to the O3 cascade strengths by assuming that the Lyα profile is flat out to O3. In this case, the O1 and O3 cascades are pumped equally, and the fluorescent line intensities are simply related to the statistical weights of the $l = 1$ and $l = 2$ sublevels: $I_{O3}/I_{O1} = 3/5$. We therefore estimate that the maximum contribution to the [Ne V] λ3426 blend from Bowen cascades (combined O3 and O1) is $0.59 I_{3133}$. This value still accounts for less than half of the residual blend intensity above, which suggests the possibility of an additional non-Bowen component.

Given the observed spectral range and resolution, we could not search for the N III Bowen lines. In Figure 3*b* we have synthesized the wide and narrow slit observations (§ II) to produce a single spectrum for ~4200–5000 Å. However, since the observed line-to-continuum flux ratio is significantly different in the wide- and narrow-slit spectra we cannot use He II λ4686, Hβ, or [O III] λ4959 as emission-line diagnostics, thus precluding determinations of the reddening and ELR density for this object.

iii) *Mrk 359*

The spectrum of Mrk 359 is contaminated by stellar absorption lines redward of ~3600 Å. In addition, the image of Mrk 359 appears extended on the Palomar Observatory Sky Survey plates. We conclude that starlight makes a significant contribution to the overall spectrum, but by using the small synthesized aperture (see § II*b*) we were able to exclude most of the stellar absorption in the regions of interest.

For this galaxy, λ3133 is strong and broad, while λ3204 has an odd profile contaminated by noise in the continuum (Fig. 2*c*). We fit the λ3204 profile with a Gaussian, using λ4686 as a fixed-width template, to calculate I_{3204}. However, given the low signal-to-noise ratio in λ3204, I_{3204} is uncertain by as much as 50%. We see evidence for λ3444, though the line intensity ($=0.11 I_{3133}$) is less than half that expected from the branching ratios. As in UM 16, the anomalously low value of I_{3426}/I_{3346} (=2.3) suggests that the O III λ3341 Bowen line is blended with [Ne V] λ3346. This line is the strongest predicted

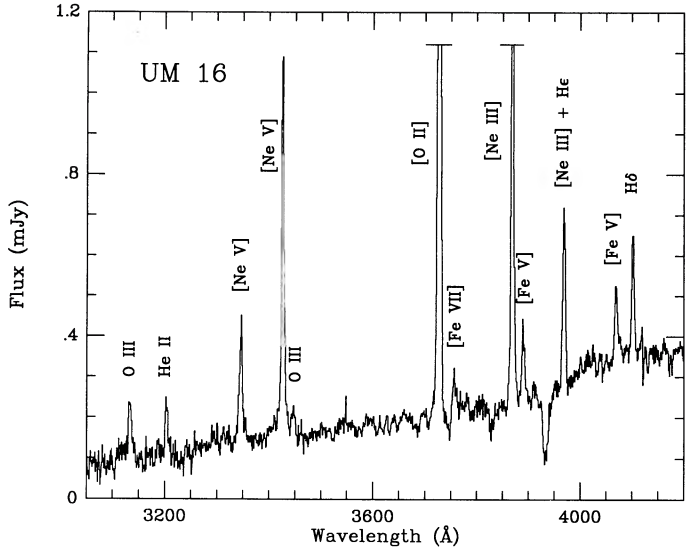

FIG. 2*a*

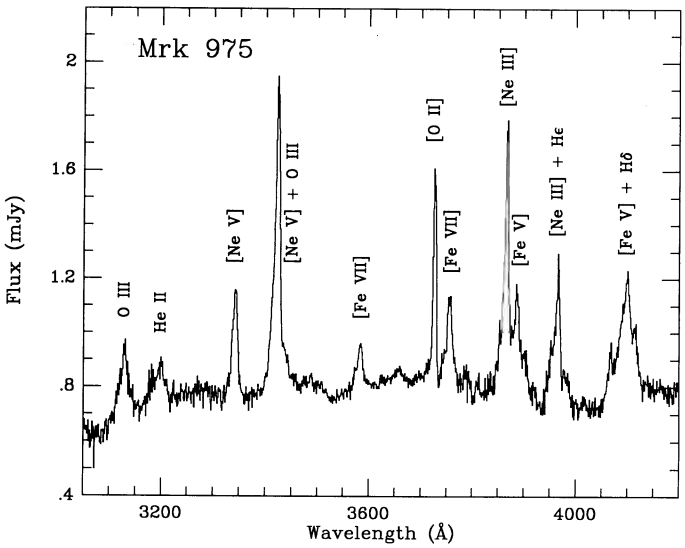

FIG. 2*b*

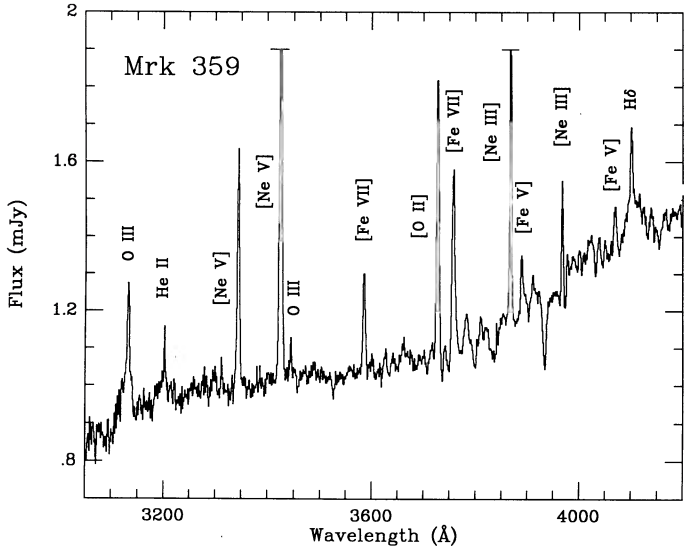

FIG. 2*c*

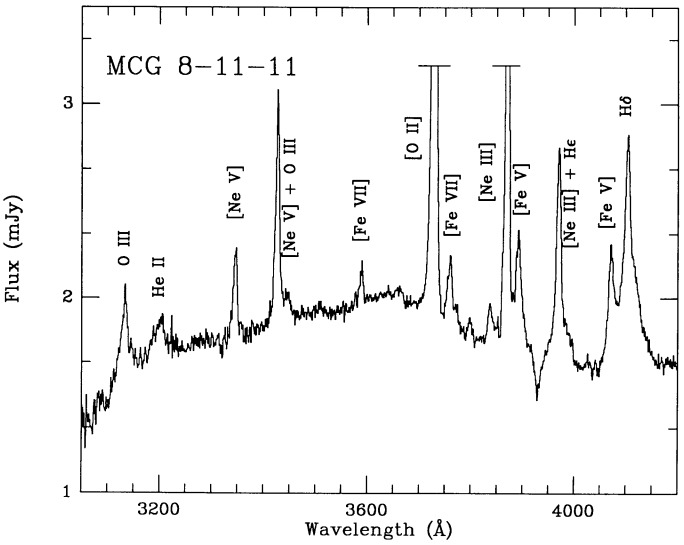

FIG. 2*d*

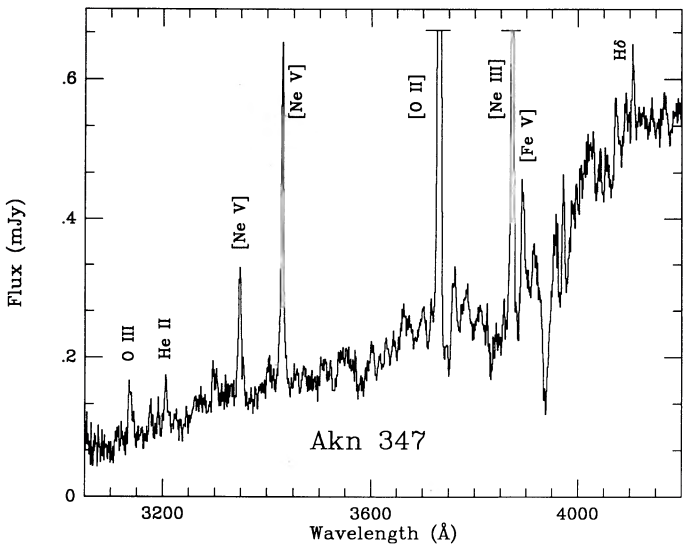

FIG. 2*e*

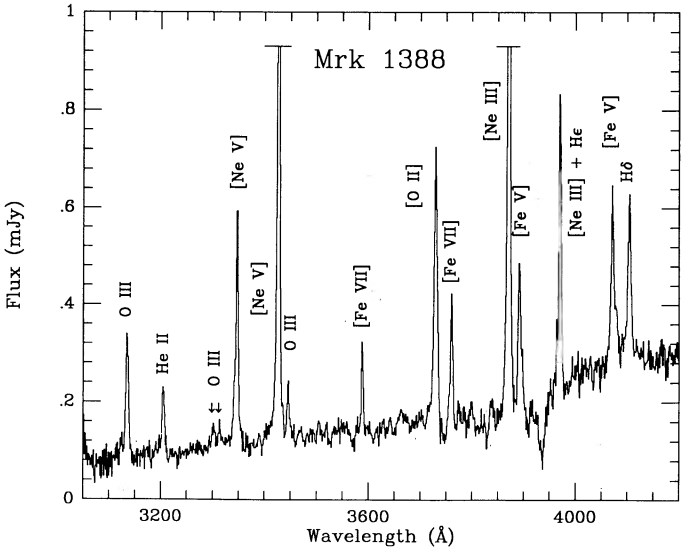

FIG. 2*f*

FIG. 2.—Spectra of program galaxies in the range 3050–4200 Å, with observed flux plotted against rest wavelength. The scale on the vertical axis has been chosen to emphasize weaker lines. Emission lines whose peaks lie above the maximum flux value are indicated with dashes. Many objects show high-ionization lines, up to [Fe VII]. Cases of clearly detected Bowen lines (also see § III*a*) are (*a*) UM 16, λλ3133, 3444; (*b*) Mrk 975, λ3133; (*c*) Mrk 359, λλ3133, 3444; (*d*) MCG 8-11-11, λλ3133, 3444; (*e*) Akn 347, λ3133; (*f*) Mrk 1388, λλ3133, 3299, 3312, 3444; (*g*) III Zw 77, λλ3133, 3444; (*h*) Mrk 1126, λλ3133, 3444. [Fe V] λ4071 may be contaminated by [S II] λλ4069, 4076 in (*b*), (*d*), and (*f*).

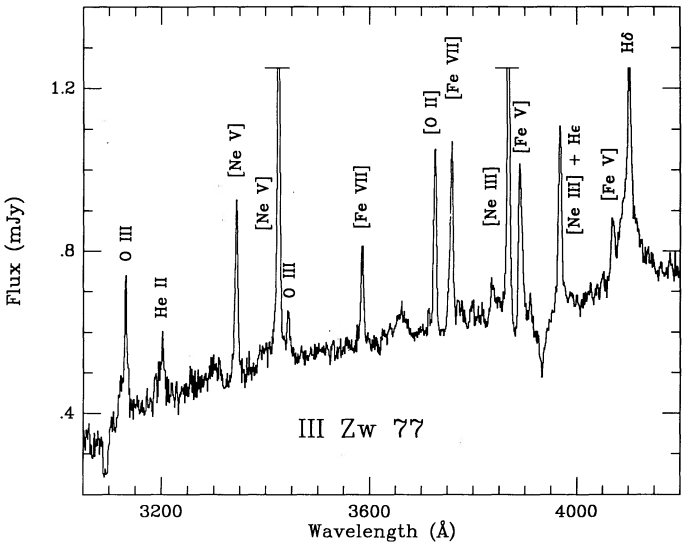

FIG. 2g

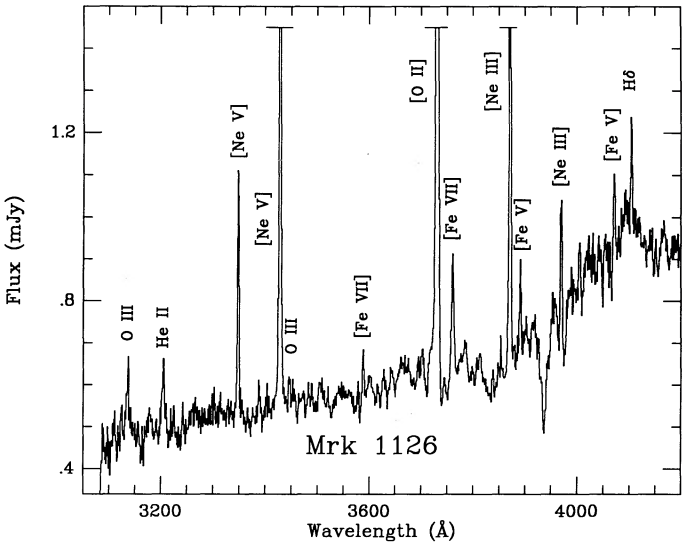

FIG. 2h

cascade following emission of λ3133. We may derive an approximate value for I_{3341} from equation (1). This approach yields $I_{3341}/I_{3133} \approx 0.21$, 50% higher than the predicted value.

A faint bump spanning the range 4600–4650 Å (Fig. 3*c*) may contain the N III λλ4634, 4641, 4642 Bowen lines. However, the bump probably also contains Fe II λλ4621, 4629, 4648, as suggested by the presence of other, unblended lines of multiplets 37 and 38 (Phillips 1978). Moreover, starlight is a significant contaminant in this spectral region. We quote the entire bump intensity as an crude upper limit to the nitrogen line strength (Table 3).

iv) *MCG 8-11-11*

This object possesses strong λ3133 and weaker λ3204 (Fig. 2*d*). O III λ3444 is partly blended with [Ne V] λ3426. A two-Gaussian deblending analysis, with [Ne V] λ3346 as a template, was used to separate the individual components of the blend. We find $I_{3444}/I_{3133} \approx 0.30$, which is close to the expected value.

He II λ4686 (Fig. 3*d*) has both broad (FWHM ≈ 6000 km s^{-1}) and narrow (FWHM ≈ 1000 km s^{-1}) components. The broad blue wing is blended with [Fe III] λ4657, but the N III Bowen lines are absent or extremely weak (cf. Fig. 6 of Stirpe, de Bruyn, and van Groningen 1988). The broad red wing may contain [Ar IV] λλ4711, 4740. We attempted to separate the broad and narrow He II components via a two-Gaussian fit to the observed profile. In Table 3 we note that I_{4686n} (where the subscript "n" indicates a narrow component) is approximate. The fits were poor, which suggests that the observed He II profile is not simply the sum of two Gaussians. Fe II emission, present near [O III] λλ4959, 5007, no doubt contaminates the He II region of the spectrum as well.

v) *Akn 347*

The spectrum of Akn 347 has significant stellar absorption lines. In the near-UV (Fig. 2*e*), these features slightly complicate the measurements of the [Ne V] line intensities. However, the λ3133 Bowen line and λ3204 are essentially free of absorption. For λ4686, absorption contributes to the blue wing, making the line intensity uncertain at the level of ~25%. No nitrogen Bowen lines appear to be present (Fig. 3*e*).

Shuder and Osterbrock (1981) reported the presence of λ3133 emission in Akn 347, obtaining $I_{3133}/I_{3204} = 2.4$. By comparison, we obtain 1.1 for this ratio, which is significantly lower, reflecting a smaller Bowen yield (§ IV*a*).

vi) *Mrk 1388*

In this galaxy, a blend centered near 3426 Å (Fig. 2*f*) appears to have broad and narrow components. The narrow components can be identified with [Ne V] λ3426 and O III λ3444; the broad component is centered at 3424 Å. A three-Gaussian deblending analysis, with He II λ4686 as template, was used to separate the blended components. We find $I_{3444}/I_{3133} \approx 0.32$, which is in reasonable agreement with the atomic physics predictions. However, the apparent intensity of [Ne V] λ3346 is too strong relative to the deblended narrow component of λ3426 ($I_{3426n}/I_{3346} \approx 1.7$). From equation (1) we may attempt to identify the excess intensity in λ3346 (I_{xs}) with the presence of Bowen emission; we find $I_{xs} = 0.77 I_{3133}$. The only possible Bowen candidate is λ3341, whose intensity relative to λ3133 (from eq. [1]) is about 6 times larger than the predicted value. We quote the derived I_{3341} as an upper limit in Table 3. Two other Bowen cascades, O III λλ3299, 3312, are also detected, though the signal-to-noise ratio is low, and we estimate that the derived intensities are uncertain by 50%. Together with λ3341, these lines represent all possible cascades produced after emission of a λ3133 photon (Fig. 4). However, the line strengths of λλ3299, 3312 are once again much higher (~7 and ~2 times, respectively) than the predicted values.

An explanation to consider for the enhancement of λλ3299, 3312, 3341 over the SS predictions is charge transfer (CT) of H I and O IV, which populates the ^3S level of O III. Suppose, therefore, that these cascades are anomalously strong because the rate of population of the ^3S level due to CT (CT rate) exceeds the rate from Bowen cascades (Bowen rate). We require (CT rate)/(Bowen rate) ≈ 4 to explain the data. Sternberg, Dalgarno, and Roueff (1988) show that

$$\frac{\text{(CT rate)}}{\text{(Bowen rate)}} \approx 90 \frac{I_{5592}}{I_{3133}} \qquad (2)$$

(cf. Paper I, § V*a*) where I_{5592} is the intensity of O III λ5592, a line which has a contribution from CT but not from Bowen fluorescence. Hence, we would expect that $I_{5592}/I_{3133} \approx 4$

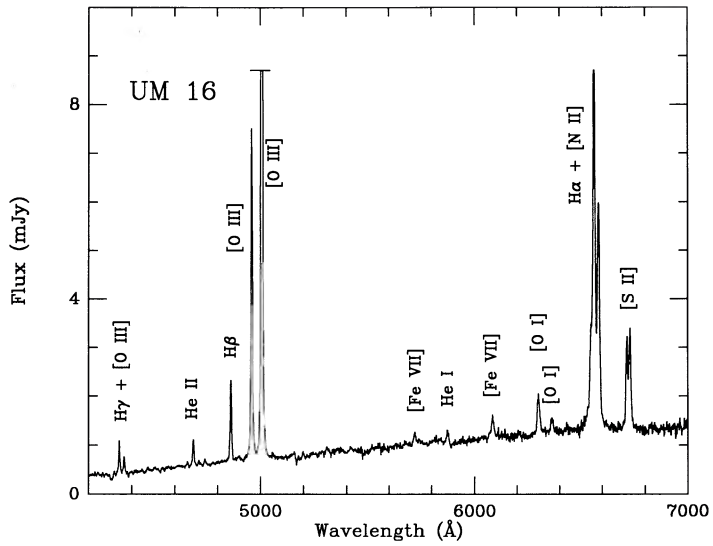

FIG. 3*a*

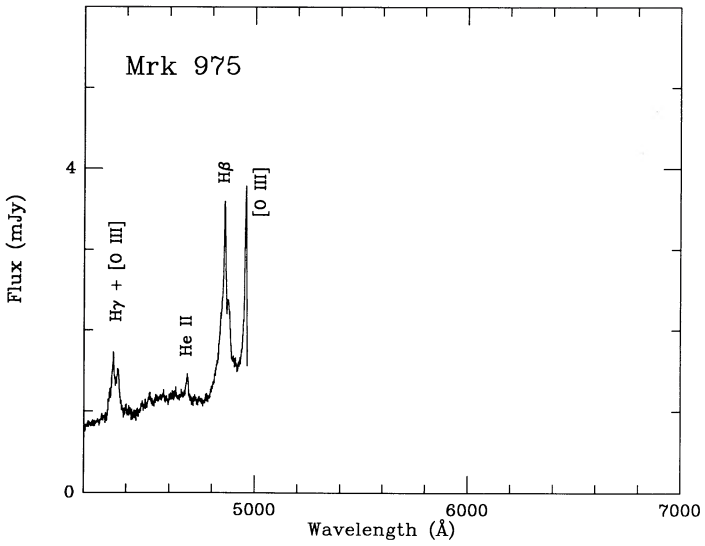

FIG. 3*b*

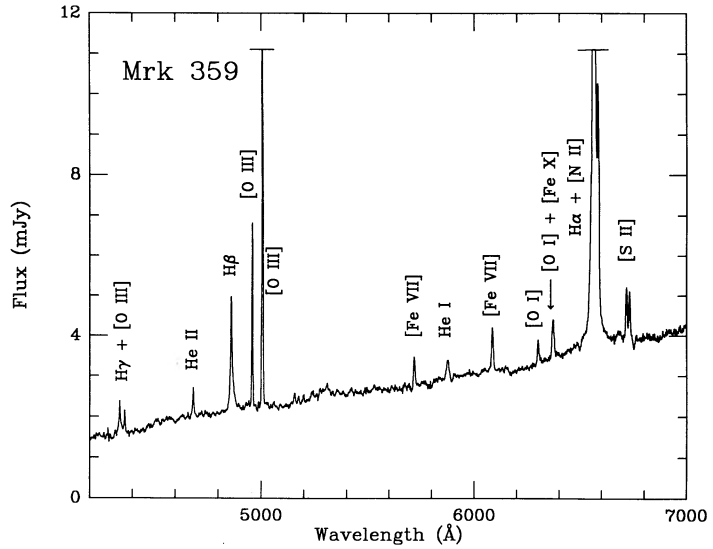

FIG. 3*c*

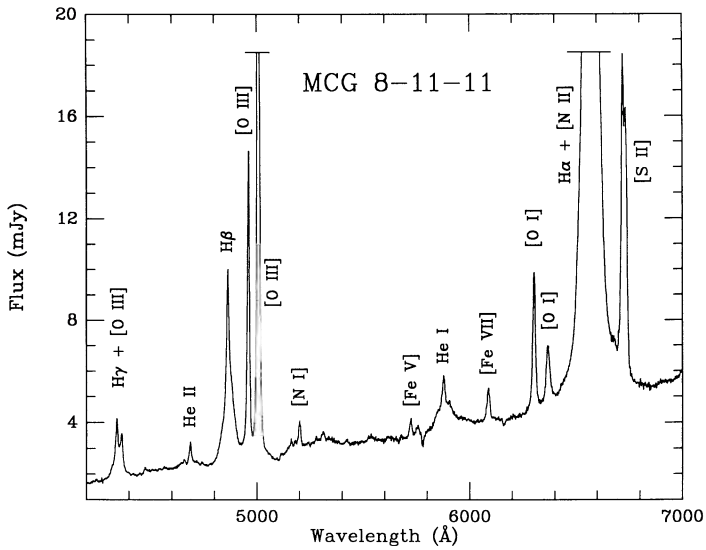

FIG. 3*d*

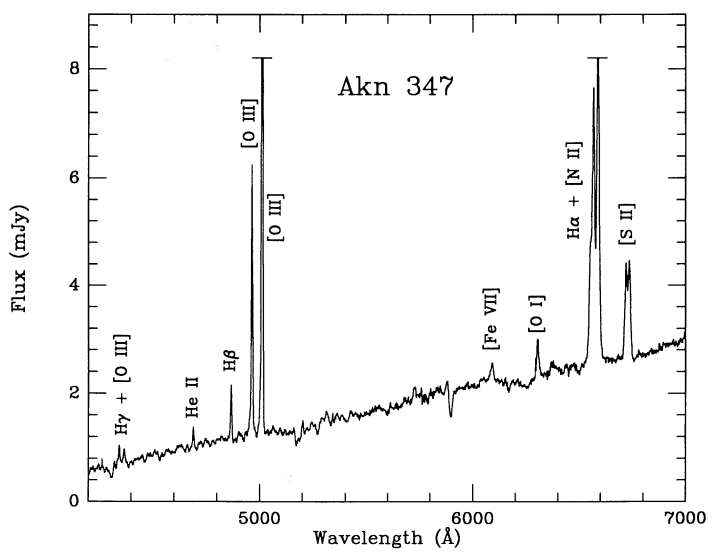

FIG. 3*e*

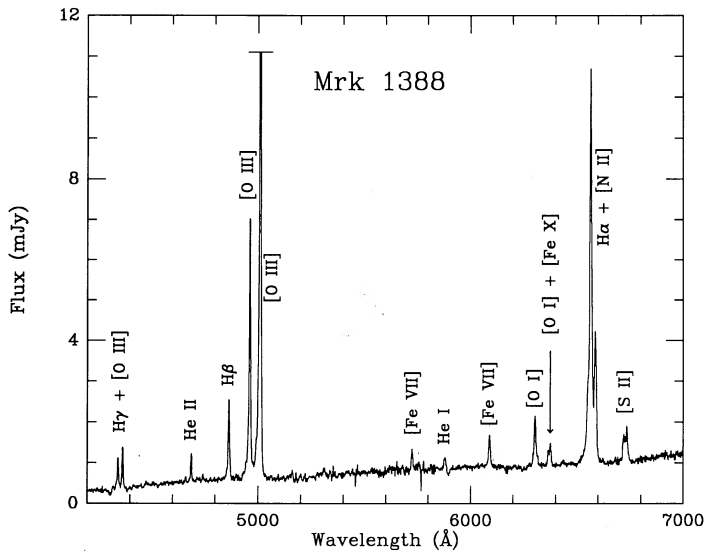

FIG. 3*f*

FIG. 3.—Optical spectra of program galaxies (4200–7000 Å, except Mrk 975, 4200–5000 Å), with observed flux plotted against rest wavelength. The spectrum of Mrk 975 is based on a synthesis of wide- and narrow-slit observations, unlike other program galaxies. All the objects show high-ionization lines (through [Fe VII]), although we note cases of unusually high ionization ([Fe X]). (*a*) UM 16. (*b*) Mrk 975; converage is incomplete, since the object was observed late in the study (§ III*a*). (*c*) Mrk 359; note presence of [Fe X]. (*d*) MCG 8-11-11. (*e*) Akn 347. (*f*) Mrk 1388; this galaxy has a small amount of [Fe X] emission. (*g*) III Zw 77; strong [Fe X] emission present. (*g*) Mrk 1126; [Fe X] emission present.

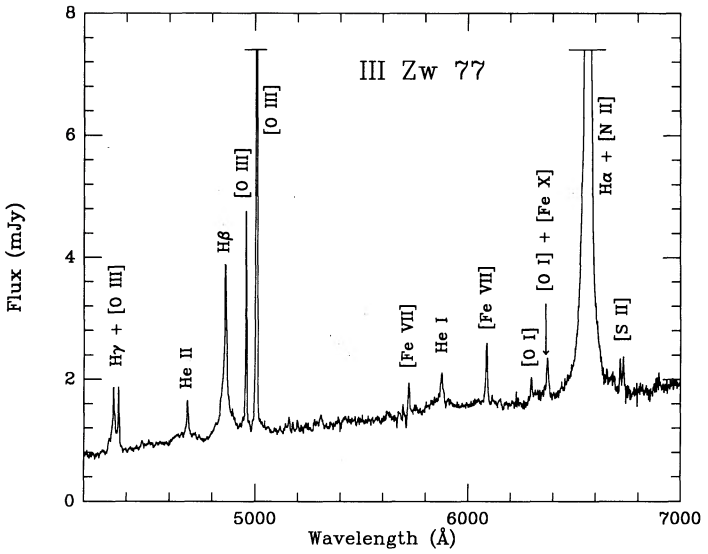

FIG. 3g

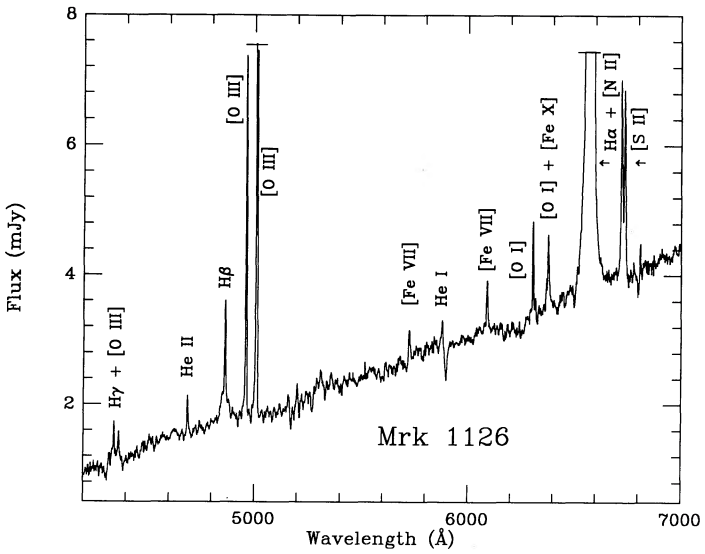

FIG. 3h

$\times 10^{-2}$. In our spectrum, we find no obvious feature near 5592 Å, but we may set an approximate upper limit of $I_{5592}/I_{3133} < 9.4 \times 10^{-3}$, after dereddening (§ IIIc). Therefore, the CT explanation is ruled out by our data.

vii) *III Zw 77*

The irregular shape of the blue wing of λ3133 (Fig. 2g) in this galaxy results from a bad column on the CCD detector. Also, the intensity of λ3204 is uncertain by ~25% because of excess noise near the blue wing. There is a broad blend consisting of [Ne v] λ3426, O III λ3444, and a broad component centered at 3413 Å. We used a three-Gaussian deblending program to separate the components, although we had difficulty fitting the 3413 Å feature (which therefore may have a non-Gaussian profile). Without the broad component, the fits are unacceptable; however, we estimate that the λ3426 and λ3444 fluxes are ~10% higher than *with* the broad component. We find $I_{3444}/I_{3133} = 0.24$, lower than the SS prediction. Our value may be compared with that obtained by Osterbrock (1981), who found $I_{3444}/I_{3133} = 0.17$, but unfortunately did not comment on the discrepancy with SS. As in the case of Mrk 1388, the observed value of I_{3426n}/I_{3346} (=2.1) is significantly less than the SS prediction of 2.7, which strongly suggests that the narrow λ3346 profile is blended with O III λ3341. Equation (1) yields $I_{3341} = 0.25 I_{3133}$, or 1.8 times the SS value. We consider this to be reasonable agreement, given the problems in fitting the broad 3413 Å feature. Unlike the situation in Mrk 1388, the O III λλ3299, 3312 cascades seem to be absent in III Zw 77, and we can probably rule out a significant contribution of charge transfer to the O III emission.

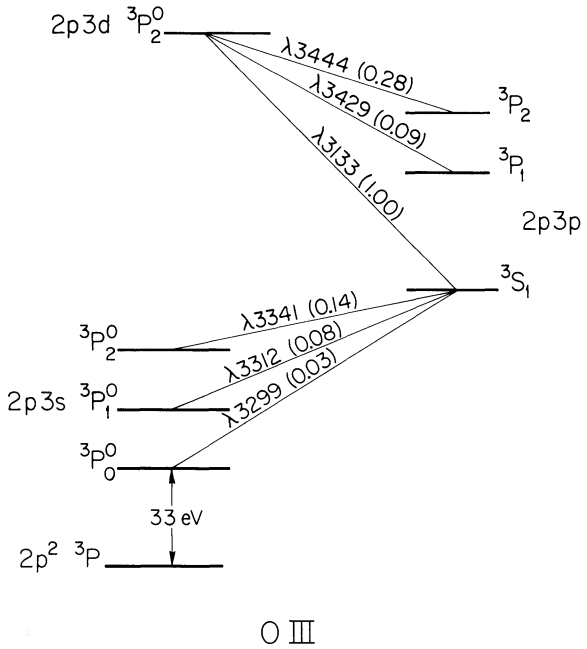

FIG. 4.—Grotrian diagram showing important transitions arising from the $2p3d\ ^3P_2^o$ level of O III. Each observable cascade is labeled by wavelength (in Å), and predicted intensity relative to I_{3133} (in parentheses; SS).

The He II λ4686 profile (Fig. 3g) contains some amount of stellar absorption, although this probably only diminishes the observed flux by ~10%. We used two Gaussians to fit the broad and narrow components of λ4686. Our method poorly fits the broad profile, so the derived narrow-line flux in this line is probably known to no better than ~20%. We see no evidence for the nitrogen Bowen lines in this galaxy.

viii) *Mrk 1126*

O III λ3444 is present (Fig. 2h), and we find $I_{3444}/I_{3133} = 0.33$, which is slightly higher than the predicted value. The measured ratio of [Ne v] lines, $I_{3426}/I_{3346} = 3.2$, is larger than the predicted value. From Figure 4 we might expect O III λ3429 to be present. Since the [Ne v] profiles appear virtually identical, we simply scaled up the λ3346 profile and subtracted it from the λ3426 profile. The residual intensity is quite noisy, although we can identify a feature near 3429 Å. However, we have $I_{3429} \approx 0.16 I_{3133}$, which is 1.7 times the SS value (similar to III Zw 77).

Stellar absorption lines in the blue and red wings of λ4686 (Fig. 3h) may have caused us to underestimate the line intensity by 10%–15%. No nitrogen Bowen lines appear to be present.

b) *Reddening Determination*

As in Paper I, we need accurate knowledge of the extinction to calculate the He II Lyα luminosity. The principal means of

determining the reddening will be from the requirement that I_{3204}/I_{4686} match the value expected for case B recombination of He II. For $T = 10^4$ K and $10^4 \leq n_e \leq 10^6$ cm^{-3} (anticipating § IIIc), $I_{3204}/I_{4686} = 0.41$–0.43 (Hummer and Storey 1987). We adopt the value 0.42, although choosing 0.41 or 0.43 would merely shift the reddening values by a small amount ($E_{B-V} = 0.015$). A standard interstellar extinction curve (Seaton 1979) gives

$$E_{B-V} = 1.77 \log \left[\frac{0.42}{I_{3204}/I_{4686}} \right]. \quad (3)$$

(Note that all logarithms used are with respect to base 10.) For each object we may check the derived value of E_{B-V} by comparison with that obtained from the H I Balmer decrement:

$$E_{B-V} = 2.07 \log \left[\frac{I_{H\alpha}/I_{H\beta}}{3.1} \right]. \quad (4)$$

We use 3.1, rather than the case B value of 2.86, for $I_{H\alpha}/I_{H\beta}$ because collisional excitation of Hα is important in the narrow-line regions of AGNs (Halpern and Steiner 1983).

Problems arise in applying both methods to the sample objects. The reddening determination for III Zw 77 deserves special note. For this case, the measured I_{3204}/I_{4686} ratio *exceeds* that predicted by case B recombination with no reddening.[6] (Of the other sample galaxies, only MCG 8-11-11 shows this behavior, and the discrepancy is probably due to an undermeasurement of I_{4686n}; § IIIa.) This curious result, echoed in Osterbrock (1981), suggests that the He II Paschen lines are optically thick in III Zw 77. However, another He II reddening indicator—I_{1640}/I_{4686}, where I_{1640} is the intensity of He II λ1640 (Balmer α)—is available. From nearly simultaneous *International Ultraviolet Explorer* (*IUE*) and optical spectra, Ferland and Osterbrock (1987) found that $I_{1640}/I_{4686} = 8.8$. This ratio is larger than the case B value of 7.6, but Ferland and Osterbrock cite AGN photoionization calculations in which I_{1640}/I_{4686} can be as large as 10 (Netzer, Elitzur, and Ferland 1985). If we adopt 10 as a strict upper limit for the line ratio, then $E_{B-V} < 0.03$, where we have again used the extinction curve in Seaton (1979).[7] Our observed value of I_{4686} is ~20% lower than that of Ferland and Osterbrock, where the discrepancy is probably caused by measurement errors. With the *IUE* I_{1640} value, we find $I_{1640}/I_{4686} = 11$.

We can also set reddening constraints for III Zw 77 using the H I lines. In general, these give higher values of E_{B-V} than the He II lines. Our observed profiles of Hα, Hβ, Hγ, and Hδ all possess both broad and narrow components, although separation of the two components is difficult. The Hγ intensity is especially uncertain because of contamination with [O III] λ4363 emission and G-band absorption. From $I_{H\alpha}/I_{H\beta}$ and $I_{H\delta}/I_{H\beta}$, we obtain $E_{B-V} \approx 0.5$–0.6. By contrast, Ferland and Osterbrock (1987) obtain $E_{B-V} < 0.25$ from $I_{Ly\alpha}/I_{H\beta}$; nevertheless, in their calculation the broad component of Hβ was not removed. If the H I zone contains more dust than the O III (and He II) zone in narrow-line Seyfert 1 nuclei (as suggested by Goodrich 1989), the intrinsic reddening should be larger in the H I zone. In this case, we would expect to find larger reddening values from $I_{H\alpha}/I_{H\beta}$ than from I_{3204}/I_{4686}. Since the Bowen lines are likely to be produced in the He II zone, we adopt the value $E_{B-V} = 0.03$ derived from I_{1640}/I_{4686}.

We now consider the other objects in our sample. In Mrk 359, the λ3204 line intensity is uncertain enough that the Balmer decrement method is more appropriate. In MCG 8-11-11, I_{3204}/I_{4686} exceeds its case B value, so we can only calculate E_{B-V} from the H I lines. Both of these objects, however, possess Balmer lines (Hα, Hβ, Hγ, Hδ) with both broad and narrow components, as do Akn 347 (Hα only), Mrk 1388 (Hα and Hβ), and Mrk 1126 (Hα, Hβ, Hγ, Hδ). Since the Bowen lines are probably produced in the narrow-line region, the ratio of narrow components, $I_{H\alpha n}/I_{H\beta n}$, should be used to calculate E_{B-V}. We used a two-Gaussian deblending program to separate broad and narrow Hβ, and a three-Gaussian deblending program (four-Gaussian in the cases of broad Hα) to separate Hα from the individual [N II] lines. The fits were usually good, except for Mrk 1126, where stellar absorption is a contaminant. For this galaxy, the Balmer line fluxes are only approximate, as is the value of E_{B-V} derived from the Balmer decrement.

Our final reddening estimates are given in Table 4. In the four objects for which we can use both techniques of reddening determination, the agreement is reasonable. The Bowen process, if it is present at all, must take place in the He II zone. Therefore, we adopt the He II–derived reddening for all objects to which it can be applied—UM 16, Akn 347, Mrk 1388, III Zw 77 (from I_{1640}/I_{4686}), and Mrk 1126. For Mrk 359 and MCG 8-11-11, on the other hand, we use reddening values derived from the Balmer decrement.

c) *Density Determinations*

In this subsection we derive estimates of the electron density (n_e) from observed line ratios; we discuss the density of the Bowen ELR in a later section (§ IVd). The [S II] I_{6716}/I_{6731} line ratio is traditionally used to estimate n_e in Seyfert nuclei (Osterbrock 1989). This approach typically yields $n_e \approx 10^3 (T_e/10^4 \text{ K})^{-1/2}$ cm^{-3}. However, densities in the [O III] zone, the likely site of Bowen emission (§ IVd), could be significantly higher than the [S II] values in our sample of galaxies (10^4–10^6 cm^{-3}). This conclusion comes from the observed [O III] $(I_{5007} + I_{4959})/I_{4363}$ line ratio (hereafter r_O). Based on r_O, we may divide the program galaxies into two groups: (1) those with $r_O \approx 40$–100 (UM 16, Akn 347, Mrk 1388, and Mrk 1126, hereafter the *Rare Group*) and (2) those with $r_O \approx 10$–30 (Mrk 359, MCG 8-11-11, and III Zw 77; hereafter the *Dense Group*). In the Rare Group, the electron temperatures derived from r_O in the low-density limit (Osterbrock 1989, eq. [5.4]) are consistent with a photoionized NLR (Halpern and Steiner 1983). Thus, we might expect that $n_e = 10^3$ cm^{-3} in the [O III] zone, as in the [S II] zone. However, the [O III] zone density could be considerably higher ($n_e \lesssim 4 \times 10^4$ cm^{-3}) and still appear to be in the low-density limit, given typical measurement uncertainties (§ IIIa). By allowing the actual value of r_O to be 80% of its observed value, we may set an approximate upper limit on the [O III] density at the calculated T_e.

For the Dense Group objects, the calculated T_e values from r_O in the low-density limit are too large (27,000–79,000 K) for a photoionized NLR, indicating that high densities are present

[6] All line intensities used for reddening determination of III Zw 77 are narrow components.

[7] As noted in Paper I, reddening values derived from I_{1640}/I_{4686} are strongly dependent on the choice of an optical-UV extinction curve. We have therefore used the standard Seaton (1979) tabulation. Ferland and Osterbrock (1987) derive $E_{B-V} < 0.1$, a less stringent upper limit for the reddening, from $I_{1640}/I_{4686} = 8.8$; however, the authors did not mention the extinction curve used.

TABLE 4

PHYSICAL CONDITIONS

OBJECT	E_{B-V}		log n_e		T_e:			
	He II[a]	Hα/Hβ[a]	[S II][b]	[O III][b]	[O III][c]	y_{HeO}	log τ_4	$x_\odot$[d]
UM 16	0.13	0.17	2.85	<4.57	1.4	0.19	0.04	0.24
Mrk 975	...	...	...	...	...	0.15	0.19	0.14[e]
Mrk 359	0.23[f]	0.65	1.60	6.21	7.9	0.49	1.16	0.07
MCG 8-11-11	[f]	0.90	2.30	5.86	3.6	0.29	0.40	0.16
Akn 347	0.02	0.17	2.81	<4.86	1.9	0.14	0.23	0.12
Mrk 1388	0.07	0.09	2.53	<4.68	1.8	0.23	0.41	0.12
III Zw 77	0.03[g]	0.59:	2.70	5.66	2.7	0.27	0.79	0.06
Mrk 1126	0.09	0.40:	2.67	<3.83	1.3	0.12	0.01	0.18

[a] Units are magnitudes. E_{B-V} from He II refers to I_{3204}/I_{4686} method, except for III Zw 77 (see § IIIb).
[b] Density is in cm^{-3}, with upper limits as noted.
[c] Low-density limit. Units are 10^4 K.
[d] Metallicity relative to solar.
[e] Adopted metallicity is the average of those of the other seven objects.
[f] I_{3204} uncertain.
[g] He II E_{B-V} value from I_{1640}/I_{4686}; see § IIIb.

in the [O III] zone. From the tables of Filippenko and Halpern (1989), we may estimate the density from the observed r_O values by requiring that $T_e = 15{,}000$ K. We now discuss our methods for determining the line ratios from the data.

Table 4 lists n_e values for the sample objects derived from [S II]. We converted I_{6716}/I_{6731} to a density from the tables in Filippenko and Halpern (1989), taking $T_e = 15{,}000$ K. We used a two-Gaussian deblending program to separate the individual [S II] components. In some objects the fits were slightly affected by the presence of faint, broad Hα emission (MCG 8-11-11, Akn 347, III Zw 77) or by nearby stellar absorption (Mrk 359, Mrk 1126). However, in no case is the derived density sensitive to these effects. Mrk 1388 has a spurious emission feature, most likely a cosmic ray, present at the center of the [S II] doublet. For this object, we adopt the [S II] ratio from Osterbrock (1985). In III Zw 77, where [S II] λ6731 has a noisy red wing, the fit was poor; nevertheless, we estimate that the inferred [S II] density for this galaxy is uncertain by a factor of 2 at most (in good agreement with Ferland and Osterbrock 1987).

Also listed in Table 4 are the densities (including the Rare Group upper limits; see § IVd) derived from [O III]. In addition, we quote the electron temperatures of all the sample galaxies in the low-density limit. A two-Gaussian deblending analysis was used to separate [O III] λ4363 from Hγ in Mrk 359, MCG 8-11-11, and Akn 347. The fit was poor in Mrk 359 because of weak, broad Hγ emission. In MCG 8-11-11, we first subtracted a scaled estimate of the broad Hβ profile from [O III] + Hγ. A small broad component still remained, so we deblended the narrow components of Hγ and λ4363. Also, in this galaxy λλ4959, 5007 appear to have both broad and narrow components. The values of I_{4959} and I_{5007} come from Gaussian fits to the narrow components, which account for ~90% of the total line flux in both cases. In Mrk 1388 and Mrk 1126, strong G-band absorption makes deblending difficult, but it is possible to estimate the values of I_{4363} in both galaxies to better than a factor of 2. In III Zw 77, the [O III] fluxes are approximate in view of the strong, broad Hγ and Hβ profiles.

IV. DISCUSSION

a) Derived Bowen Yields

The oxygen fluorescence yield is given by

$$y_{HeO} = \frac{I_{O\,III}}{I_{He\,II}} \frac{\lambda_{O\,III}}{\lambda_{He\,II}} \frac{\alpha_{eff}(\lambda_{He\,II})}{\alpha_{eff}(Ly\alpha)} \frac{P(O\,III\ 2p3d \rightarrow 2p3p)}{P(\lambda_{O\,III})}, \quad (5)$$

where $\lambda_{O\,III}$ and $\lambda_{He\,II}$ are wavelengths of the observed emission lines of O III and He II, α_{eff} is the effective recombination coefficient, $P(O\,III\ 2p3d \rightarrow 2p3p)$ is the total emission probability from the O III $2p3d$ level (Fig. 4), and $P(\lambda_{O\,III})$ is the $\lambda_{O\,III}$ line-emission probability. We now express y_{HeO} in the useful form $y_{HeO} = k_{HeO} I_{3133}/I_{3204}$, where k_{HeO} contains all of the important atomic physics. With O III λ3133 and He II λ4686 as the two wavelengths, we take the quantities $\alpha_{eff}(\lambda 4686)$, $\alpha_{eff}(Ly\alpha)$, and I_{3204}/I_{4686} from Hummer and Storey (1987, hereafter HS), and transition probabilities from SS. This gives

$$y_{HeO} = 0.12 \frac{I_{3133}}{I_{3204}} \quad (6)$$

for $T = 1.5 \times 10^4$ K and $10^2 \leq n_e \leq 10^7$ cm^{-3}. The value of k_{HeO} does not vary appreciably over the range $T_e = 1.0 \times 10^4$ to 2.0×10^4 K.[8]

As outlined in Paper I, observations of y_{HeO} may be used to set limits on τ_L. We refer to Figure 5 of KM80, in which y_{HeO} is plotted as a function of τ_L. In KM80, τ_L is expressed in units of τ_{crit}, which is the point at which He II Lyα escape and Bowen conversion are equally likely. The value of τ_{crit} depends on the ratio of helium to oxygen ion fractions in the Bowen region: $\tau_{crit} \approx 70\, n_{He\,II}/n_{O\,III}$ (correction of "$80\, n_{He\,II}/n_{O\,III}$" in KM80;

[8] Eastman and MacAlpine (1985) argued that for $n_e \gg 10^6$ cm^{-3} and $T = 2.0 \times 10^4$ K, l-state redistribution will decrease the ratio $\alpha_{eff}(\lambda 4686)/\alpha_{eff}(Ly\alpha)$. They predicted that $k_{HeO} \approx 0.085$ under such conditions. This result is inconsistent with HS, who explicitly include the effects of l-state redistribution on the effective recombination coefficients. Using HS yields $k_{HeO} = 0.11$ at densities as high as 10^{10} cm^{-3}. We adopt the HS calculations, and find that k_{HeO} decreases only slightly (~8%) over a wide range of n_e values (10^2–10^{10} cm^{-3}).

Kallman 1989). For $\log(\tau_L/\tau_{crit}) \leq 2$, the dependence of y_{HeO} on τ_L is approximately linear. However, y_{HeO} saturates at large opacities, when photoelectric absorption by neutral species is the only process competing with Bowen conversion.

In Sco X-1, we concluded that the observed y_{HeO} was consistent with the saturated portion of the y_{HeO} curve. However, for the present sample of Bowen Seyfert nuclei, the observed y_{HeO} values are smaller than in Sco X-1. The yields lie on the linear portion of the curve, where we find from Figure 5 of KM80 that

$$\log(\tau_L/\tau_{crit}) \approx 1.95 y_{HeO} - 0.88 . \quad (7)$$

To calculate the τ_L values, we need to know the ionic ratio $n_{He\,II}/n_{O\,III}$ at the He III front, for which photoionization calculations (see § IV*c*) invariably give a value close to the scaled solar abundance ratio. In other words, $n_{He\,II}/n_{O\,III} \approx (8.3 \times 10^{-3} x_\odot)^{-1}$, where $x_\odot$ is the metallicity relative to solar. Thus, $\tau_{crit} = 8.4 \times 10^3/x_\odot$. Introducing the notation $\tau_4 = \tau_L/10^4$, we provide the derived Bowen yields and τ_4 values in Table 4. In calculating τ_4, we have anticipated the values of $x_\odot$ derived later (§ IV*d*).

b) Single-Cloud Bowen ELR Models

In Paper I, we modeled the Bowen-emitting region as a spherical cloud characterized by a radius (R_B; the subscript denotes Bowen ELR) and electron density (n_e). We then solved for R_B and n_e using two conditions. First, the definition of τ_L is

$$\tau_L = n_{He\,II}\sigma_L R_B , \quad (8)$$

where σ_L is the (hydrogenic) He II Lyα absorption cross section. Second, the luminosity in λ4686 is given by

$$L_{4686} = 4\pi D^2 I_{4686} = \alpha_{eff}(\lambda 4686) n_e n_{He\,III} \tfrac{4}{3}\pi R_B^3 h\nu_{4686} , \quad (9)$$

where D is the distance to the source and $\alpha_{eff}(\lambda 4686)$ is the effective λ4686 recombination coefficient (from HS). We expressed $n_{He\,II}$ and $n_{He\,III}$ in terms of n_e as $n_{He\,II} = n_e/10x_{e10}$ and $n_{He\,III} = x_{He\,III} n_{He\,II}$, which defines x_{e10} and $x_{He\,III}$. The values of the ion fractions can be taken from a model calculation. For Sco X-1 we found $n_e \approx 10^6$–10^{10} cm^{-3}, $R_B \approx 10^{11}$–10^{14} cm. If this approach is adopted for the Seyfert galaxies, the results are

$$R_B \approx 2.8 \times 10^{31} \frac{I_{12} z^2}{\tau_4^2 x_{He\,III} x_{e10}} \text{ cm} \quad (10a)$$

and

$$n_e \approx 1.2 \times 10^{-13} \frac{x_{He\,III} x_{e10}^2 \tau_4^3}{I_{12} z^2} \text{ cm}^{-3} , \quad (10b)$$

where $I_{12} = I_{4686}/(12 \times 10^{-14}$ ergs cm^{-2} s^{-1}) and z is the redshift. Model calculations invariably give $x_{He\,III} = 1.0$ at the He III front, while typically $x_{e10} \approx 2$ there. We have assumed $H_0 = 100$ km s^{-1} Mpc^{-1}. Also, we have taken $T_e = 15{,}000$ K to evaluate $\alpha_{eff}(\lambda 4686)$. Using the deduced τ_4 values (Table 4) yields estimates of n_e and R_B which are clearly unreasonable ($R_B \approx 10^{26}$ cm; $n_e \approx 10^{-7}$ cm^{-3}), indicating that the assumption of a single spherical cloud is incorrect.

c) Multiple Clouds: General

The extremely low density derived for the single-cloud model suggests that the emitting gas may be highly clumped. We therefore suppose that a large number (N_c) of spherical clouds of radius r_c fill a fraction f_V of the emitting volume ($V = 4\pi R_{em}^3/3$):

$$f_V V = N_c \tfrac{4}{3}\pi r_c^3 . \quad (11)$$

By analogy with the BLR (Osterbrock and Mathews 1986), typical λ3204 line widths of $\sim$1000 km s^{-1} and thermal Doppler widths of $\sim$6 km s^{-1} imply a lower limit of $\sim$200 clouds. With the definitions above, we find

$$r_{13} = 2.7 \times 10^5 \frac{z^2 I_{12}}{\tau_4^2 N_{13} x_{e10}} , \quad (12a)$$

$$n_{e5} = 1.2 \times 10^{-5} \frac{\tau_4^2 N_{13} x_{e10}^2}{z^2 I_{12}} , \quad (12b)$$

and

$$f_{-3} R_{19}^3 = 2.0 \times 10^{14} \frac{z^6 I_{12}^3}{\tau_4^6 N_{13}^2 x_{e10}^3} , \quad (12c)$$

where $N_{13} = N_c/10^{13}$, $n_{e5} = n_e/10^5$ cm^{-3}, $f_{-3} = f_V/10^{-3}$, and $R_{19} = R_{em}/10^{19}$ cm. A summary of symbols commonly used in the text is given in Table 5.

Two additional conditions are required to close the system of equations. To this end, we have available constraints on n_e and R_{em}. The electron densities derived from forbidden-line ratios can be applied to the Bowen ELR (see § IV*d*). For the R_{em} constraint, we first need to analyze the photoionized region more carefully. Assuming that the ensemble of clouds is approximately spherical, we may distinguish two limiting cases: optically thin and optically thick photoionized regions (e.g., Kallman and McCray 1982, hereafter KM82, § IV*b*). In a standard photoionization model, the radiation field decreases with distance (r) from the source as r^{-2}. One may therefore define the *recombination radius* (R_i) at which the per-ion rates of photoionization and recombination for ion i are equal. In an *optically thin* model, the ion i recombines for $r > R_i$. The ion-

TABLE 5

COMMONLY USED SYMBOLS

Symbol	Definition	Scaled Symbol
f_V	Filling factor of clouds	$f_{-3} = f_V/10^{-3}$
I^c_{3300}	Monochromatic 3300 Å intensity, extinction corrected and de-redshifted	$I_{c1} = I^c_{3300}/(10^{-26}$ ergs cm^{-2} s^{-1} Hz^{-1})
I_{4686}	Intensity of λ4686, extinction corrected and de-redshifted	$I_{12} = I_{4686}/(12 \times 10^{-14}$ ergs cm^{-2} s^{-1})
n_e	Electron density	$n_{e5} = n_e/10^5$ cm^{-3}
N_c	Number of clouds	$N_{13} = N_c/10^{13}$
r_c	Cloud radius	$r_{13} = r_c/10^{13}$ cm
R_{em}	Emission region radius	$R_{19} = R_{em}/10^{19}$ cm
τ_L	Line-center Lyα opacity	$\tau_4 = \tau_L/10^4$

ization throughout the photoionized region can be characterized by a single scaling quantity (the *ionization parameter*), given by $\xi_i = L/n_g R_i^2$, where L is the ionizing luminosity and n_g is the gas density. In particular, for any value of the ionization parameter, the ionic ratios (e.g., He II/O III for our case) in *all* optically thin models should be identical. Often it is stated in the AGN literature (e.g., Stasińska 1984) that all photoionization models, whether optically thick or thin, depend solely on ξ (or something relatively similar). Of course, in a general model, only the value ξ at the irradiated face of the cloud is a proper scaling parameter. For this reason, we prefer to use the quantity ξ only in the discussion of optically thin models.

In the *optically thick* limit, the ionization may be very different. Geometric dilution of the radiation field is unimportant, since *all* photons are absorbed within the Strömgren radius. The simple scaling by ξ cannot be used. The ionization of a particular ion will be optically thin (thick) if and only if the recombination radius lies inside (outside) the Strömgren radius, R_S. With a spherical distribution of clouds of filling factor f_V, the Strömgren radius is given by a relation of the form $f_V R_S^3 \propto Q(>4\ \mathrm{Ry})$, where $Q(>4\ \mathrm{Ry})$ is the number of ionizing photons with energies greater than the He II edge.

The ionic ratios among optically thick models are generally different from the corresponding optically thin cases. However, a comparison with published models (KM82; Halpern 1982) shows that ionic ratios necessary for our analysis—$n_{\mathrm{He\,II}}/n_{\mathrm{O\,III}}$ and $n_e/n_{\mathrm{He\,II}}$ evaluated at the He III front—vary by only a small amount between optically thin and thick models over the range of physical conditions of our sample objects. In general, $n_{\mathrm{He\,II}}/n_{\mathrm{O\,III}} \approx 120$ (scaled to abundances), while $x_{e10} \approx 2$.

For our purposes, therefore, the key difference between the two cases is in the determination of R_{em}. Since the relation for R_S does not provide an independent constraint, we will initially assume that the cloud ensemble is optically thin, so that $R_{\mathrm{em}} = R_{\mathrm{He\,II}}$, where $R_{\mathrm{He\,II}}$ is the position of the He II recombination radius. We can test this assumption when the complete solution is known (§ IV*e*). Model 1 of KM82 is a representative optically thin model, for which $\xi_{\mathrm{He\,II}} = 0.63$. First, we estimate the ionizing luminosity (L) by assuming that the continuum is a power law,

$$L_\nu = L_0 \left(\frac{\nu}{\nu_0}\right)^\alpha , \tag{13}$$

where $\alpha < 0$. To normalize, we adopt the continuum value at 3300 Å (rest wavelength, hereafter, I^c_{3300}), a region of the spectrum that is featureless and largely uncontaminated by host galaxy starlight. (In any case, the derived ELR parameters are not very dependent on the continuum flux). Then, for $\alpha = -1.5$ (cf. Yee 1980) and the range of energies in the KM82 model,

$$L = 4.39 \times 10^{47} z^2 I_{c1}\ \mathrm{ergs\ s^{-1}} , \tag{14}$$

where $I_{c1} = I^c_{3300}/1$ mJy. Using $\log \xi_{\mathrm{He\,II}}$ from the model gives

$$R_{19} = 264\, \frac{z I_{c1}^{1/2}}{n_{e5}^{1/2}} . \tag{15}$$

Equations (12) and (15) are insufficient to solve for the five unknowns—r_{13}, n_{e5}, f_{-3}, R_{19}, and N_{13}. We therefore use our previously derived values of n_e (Table 4) to solve for the other four quantities in the optically thin case (§ IV*e*). First, however, we demonstrate that the density of the Bowen ELR can be estimated from observed line ratios.

d) Bowen ELR Densities

Since the density diagnostics derived in § III*c* come from ratios of forbidden-line intensities, it is germane to consider whether the (permitted) O III BF lines arise in conditions of similar densities. A variety of arguments imply that this is true. First, we expect that the site of BF is the [O III] zone, as suggested by similar profiles and widths of both the [O III] lines and Bowen lines. Second, the BF emission will arise in the He II zone, where He II Lyα is produced. A test independent of the Bowen process is provided by comparing the observed value of I_{4686}/I_{5007} with published NLR calculations (Ferland and Netzer 1983). The results are reasonably consistent for 0.1 solar metallicity. If we demand that λ4686 and λ5007 arise in the same physical region, we can constrain the metallicities further. The ratio I_{4686}/I_{5007} is given by

$$\frac{I_{4686}}{I_{5007}} = \frac{\alpha_{\mathrm{eff}}(\lambda 4686)\, n_e\, n_{\mathrm{He\,III}}\, V_{\mathrm{He\,III}}}{q(^3P_2, {}^1D_2)\, n_e\, n_{\mathrm{O\,III}}\, V_{\mathrm{O\,III}}} , \tag{16}$$

where $V_{\mathrm{He\,III}}$ and $V_{\mathrm{O\,III}}$ are the emitting volumes of gas, and $q(^3P_2, {}^1D_2)$ is the collisional excitation rate of the $^1D_2$ level, which produces λ5007. We use collision strengths averaged over the Maxwellian distribution of electrons from Eissner and Seaton (1974) to compute $q(^3P_2, {}^1D_2)$. Previously, we found that $n_{\mathrm{He\,III}}/n_{\mathrm{O\,III}} \approx 120 x_\odot$ (§ IV*c*). If both λ4686 and λ5007 come from the same physical region, then both must independently have the same n_e and same emitting volume. We can then use equation (16) to solve for the metallicity ($x_\odot$). This analysis yields $x_\odot = 0.06$–0.24 (Table 4). These values are consistent with those inferred from previous analyses of Seyfert spectra (Ferland and Netzer 1983).

Although these indirect arguments suggest that the Bowen ELR has an n_e given by the observed [O III] line ratios, we emphasize again that the BF lines are permitted; therefore, BF could conceivably be produced in regions of extremely high density (e.g., $\gtrsim 10^8$ cm^{-3}). These high-density regions, however, would be expected to produce a considerable amount of observable λ4686 emission, with no λ5007. Because we observe normal values of I_{4686}/I_{5007}, such a high-density Bowen ELR is unlikely.

In § III*c*, we divided the sample galaxies into two groups based on the inferred electron densities in the [O III] zone. For the Rare Group (UM 16, Akn 347, Mrk 1388, and Mrk 1126), we found $n_e \lesssim 4 \times 10^4$ cm^{-3} in the [O III] zone, while $n_e \approx 10^2$–10^3 cm^{-3} in the [S II] zone. Because the [O III] densities for the Rare Group are just upper limits, we adopt the full range of densities implied by these diagnostics for the remainder of the discussion. For the Dense Group (Mrk 359, MCG 8-11-11, and III Zw 77), we use the [O III] zone densities previously derived ($n_e = 10^5$–10^6 cm^{-3}).

e) Multiple Clouds: Solution

Since we have established that the electron density may be calculated from observed line ratios, we now solve the equations of § IV*c* for r_{13}, f_{-3}, and N_{13} in terms of n_{e5}. The solution is as follows:

$$r_{13} = 3.39\, \frac{\tau_4\, x_{e10}}{n_{e5}} , \tag{17a}$$

$$f_{-3} = 1.63 \times 10^{-3}\, \frac{I_{12}\, x_{e10}}{n_{e5}^{1/2}\, z\, I_{c1}^{3/2}} , \tag{17b}$$

$$N_{13} = 8.04 \times 10^4\, \frac{n_{e5}\, z^2 I_{12}}{\tau_4^3\, x_{e10}^2} . \tag{17c}$$

A comparison with equations (12) and (15) shows that the dependence of f_{-3} on τ_4 and N_{13} has vanished (since $n_e \propto \tau_4^3 N_{13}$). Thus, for a specified n_e, the filling factor of Bowen clouds is independent of $y_{\rm HeO}$. This suggests that we can calculate filling factors for general AGNs which possess He II λ4686 and a strong nonstellar continuum. (Flux-calibrated spectra and an n_e estimate would be needed.) Two other cloud parameters—r_{13} and N_{13}—do depend on τ_4, and hence on $y_{\rm HeO}$ as well. Below, we use the values of r_{13} and N_{13} to characterize the emission region in more detail.

To test whether the ensemble of clouds is in fact optically thin, we consider the general absorption of ionizing radiation by the cloud ensemble. Each cloud will absorb a portion of the ionizing luminosity at energies above 4 Ry. The optical depth for absorption in a single cloud ($\tau_{\rm indiv}$) is given by $n_{\rm He\,II}\sigma(4\ {\rm Ry})r_c$, where $\sigma(4\ {\rm Ry}) = 1.6 \times 10^{-18}$ cm^2 for He II (e.g., Osterbrock 1989). A straightforward calculation shows $\tau_{\rm indiv} = 0.54\tau_4$, so that in general with the derived τ_4 values (Table 4), the individual clouds in the sample objects are marginally optically thin. The mean number of clouds through which a photon will pass before escaping the ELR, $N_{\rm abs}$, is given by $n_c \pi r_c^2 R_{\rm em}$, where n_c is the number density of clouds ($n_c = 3N_c/4\pi R_{\rm em}^3$). The quantity $N_{\rm abs}$ is related to the covering factor. For our objects, $N_{\rm abs} \gtrsim 1$; therefore, the effective optical depth, $\tau_{\rm eff}$, for a He II–ionizing photon is given by the product $\tau_{\rm indiv} N_{\rm abs}$, or $\tau_{\rm eff} = 4.1\tau_4 N_{13} r_{13}^2 R_{19}^{-2}$. For the objects in the sample, we find $\tau_{\rm eff} > 1$. This indicates that the assumption of an optically thin photoionized region is incorrect. Nevertheless, from the discussion of § IV*c*, we know that the derived R_{19} values are upper limits; similarly, the f_{-3} values are lower limits. The values of r_{13} and N_{13} are unchanged.

For comparison, we briefly consider the optically *thick* limit for the Bowen ELR. Using the form of the ionizing luminosity discussed previously (§ IV*c*), the Strömgren radius is given by

$$\alpha_B n_e n_{\rm He\,III} f_V \frac{4}{3}\pi R_S^3 = 10^{31}\frac{I_{c1} z^2 (14.5)^\alpha}{h|\alpha|}\ {\rm s}^{-1}, \qquad (18)$$

where α_B is the case B recombination coefficient, h is Planck's constant, and α is the power-law index. Notice that equation (12c) is of the same form. The difference is that the right-hand side of equation (12c) depends on L_{4686}. Since equation (18) does not provide an independent constraint, we are unable to specify f_V or $R_{\rm em}$ uniquely. However, by demanding that equations (18) and (12c) be consistent, we can derive a relation for the power-law index: $I_{c1}/I_{12} = 6.7 \times 10^{-2}|\alpha|(14.5)^{-\alpha}$. This gives $-2.2 \leq \alpha \leq -1.5$ for the sample objects. The discrepancy with expected α-values for Seyfert nuclei ($\alpha \gtrsim -1.5$) can probably be attributed to our assumption of constant n_e throughout the cloud. In fact, much of the He III zone would be expected to have larger n_e than at the He III front. Since helium is expected to be fully ionized at the illuminated front side of the cloud, we have assumed that $n_{\rm He\,III}/n_{\rm He} = 1$ in equation (18).

In Table 6 we list the derived Bowen ELR parameters for each object; these are essentially independent of the details of photoionization. We have adopted $x_{e10} = 2$. For the Rare Group objects we calculate a range of values, corresponding to the inferred range of Bowen ELR densities. Given the uncertainty in n_e for these galaxies, the strict upper limit on the system size and the lower limit on filling factor are provided by the less restrictive values. The ELR radius ($\sim$1–10 pc) is relatively uniform. On the other hand, the cloud size ($\sim$1–1000 AU), number of clouds (10^9–10^{13}), and filling factor (10^{-3} to 10^{-7}) cover a wide range. The total cloud mass (M_c) is given by $M_c \approx N_c(4/3)\pi r_c^3 n_{\rm H} m_{\rm H}\mu$, where $n_{\rm H}$ and $m_{\rm H}$ are the total (ionized + neutral) hydrogen density and hydrogen atom mass, and $\mu \leq 1.3$ for the derived metallicities (0.06–0.24$x_\odot$; § IV*d*). We find $M_c \leq 4.4 r_{13}^3 n_{\rm H5} N_{13}\ M_\odot$, where $n_{\rm H5} = n_{\rm H}/10^5$. Using $n_{\rm H}/n_e$ from the KM82 model, we obtain $M_c = 100$–10^6 $M_\odot$ (Table 6).

Our derived size and mass may be compared with other NLR estimates. The calculated ELR radius is smaller than for canonical NLRs ($\sim$100–1000 pc in resolved Seyfert nuclei). The mass of the NLR has traditionally been calculated from the narrow-line Hβ luminosity (e.g., Osterbrock 1989),

$$M_{\rm H\beta} \approx 39\left(\frac{L_{\rm H\beta}}{n_e}\right)\left(\frac{T}{15{,}000\ {\rm K}}\right), \qquad (19)$$

with $M_{\rm H\beta}$ and $L_{\rm H\beta}$ in solar units. For our program galaxies, values of $M_{\rm H\beta}$ are in good agreement with the M_c values, differing by a factor of $\sim$2 at most. The discrepancy suggests that the H I zone has a different temperature and density than the He II zone. Interestingly, the derived cloud parameters (except n_e) are not too different from typical BLRs, where $r_{13} = 0.1$ and $N_{13} = 10^{-2}$ at $n_e = 10^{10}$ cm^{-3} (Osterbrock and Mathews 1986).

We may also calculate other physical parameters of the ELR. The cloud covering factor is given by $f_A = 1 - (\exp\tau_{\rm eff})$. We find $f_A \approx 1$ for all the galaxies, so that the path of a Lyα photon through the NLR may cross many clouds. Similar behavior for continuum photons was discussed above, where we found that the effective optical depth for the total cloud ensemble could be large compared with a single cloud. We might therefore expect that a Lyα photon escaping one cloud could be reabsorbed and reemitted by successive clouds, until

TABLE 6

DERIVED PARAMETERS FOR ELR MODEL[a]

Object	r_{13}	f_{-3}	R_{19}	N_{13}	$M_c/M_\odot$
UM 16	2.0(+1)–1.1(+3)	>6.6(−2)–4.8(−1)	<13–92	1.7(+0)–3.3(−2)	2.0(+4)–1.0(+6)
Mrk 359	6.1(+0)	>3.6(−4)	<5.1	2.3(−2)	3.2(+2)
MCG 8-11-11	2.4(+0)	>1.1(−4)	<22	9.0(+0)	3.3(+3)
Akn 347	1.6(+1)–1.8(+3)	>1.0(−1)–1.1(+0)	<2.6–27	4.5(−2)–4.0(−4)	5.2(+2)–5.8(+4)
Mrk 1388	3.6(+1)–5.1(+3)	>3.0(−1)–3.6(+0)	<3.0–36	1.8(−2)–1.3(−4)	1.6(+3)–2.3(+5)
III Zw 77	9.1(+0)	>7.3(−3)	<3.2	3.4(−2)	4.4(+2)
Mrk 1126	1.0(+2)–1.5(+3)	>1.2(−1)–4.4(−1)	<9.2–35	8.5(−3)–5.9(−4)	2.5(+3)–3.5(+4)

[a] Definitions of parameters are in § IV. Numbers in parentheses indicate powers of 10. For the Rare Group Seyferts, a range of values is given. The first value corresponds to the upper limit to n_e determined from observed [O III] line ratios, whereas the second value corresponds to n_e from [S II] line ratios. Note that these considerations imply that firm upper and lower limits for f_{-3} and R_{19} are always given by the less restrictive value.

finally being converted into a Bowen line or escaping the entire emission region. In the Doppler core, Bowen conversion dominates the transfer (KM80). Thus, the photon must diffuse in frequency away from the Doppler core in order to escape from the cloud in which it was created. Additional clouds can reabsorb the photon only if bulk velocity gradients large enough to influence the line transfer exist.

The derived values of τ_4 enable us to find the He II column density ($N_{\rm He\,II}$), via $N_{\rm He\,II} = 3 \times 10^{17}\tau_4$ cm^{-2}. Then, using ion fractions from KM82 model 1, $N_{\rm H} = 4 \times 10^{18}\tau_4$ cm^{-2}. The soft X-ray opacity is dominated by K-shell photoionization of oxygen and carbon, so it is more appropriate to quote the *equivalent hydrogen column* required to produce the same absorption. This approach yields an equivalent $N_{\rm H}$ at the oxygen K-edge of $\sim 3 \times 10^{18}\tau_4$ cm^{-2}, with 0.1 solar abundances assumed. We may compare the derived column densities with previously derived constraints. The only known X-ray source in our sample is MCG 8-11-11, for which Petre *et al.* (1984) found no evidence of intrinsic absorption, with an upper limit of 2.8×10^{21} cm^{-2} (the Galactic contribution). The column densities we have derived are considerably lower than those required to produce the observed low-ionization ([S II], [O I]) emission-line intensities (10^{21}–10^{23} cm^{-2}) in semi-infinite slab model NLR calculations (e.g., Halpern and Steiner 1983). The slab geometry is at best an idealization. However, the discrepancy between our derived parameters and the models suggests that, at least in our Dense Group Seyferts, the Bowen lines are produced in a population of low column density, high n_e clouds. Presumably, another cloud population produces [S II] and perhaps other low-ionization emission lines.

Although the sample size is small (two Seyfert 2s and six Seyfert 1s), and biased toward objects with favorable Bowen characteristics, we may make some general statements about the differences between Seyfert 2s and Seyfert 1s evident in our analysis. First, it appears that our $y_{\rm HeO}$ values for Seyfert 2s (0.14–0.19) are smaller than for Seyfert 1s (0.15–0.49). This result is in agreement with observations of Malkan (1986). Second, the filling factor and total cloud mass of the Bowen ELR seem to be larger for Seyfert 2s than for Seyfert 1s, whereas the equivalent hydrogen column is lower in Seyfert 2s than in Seyfert 1s.

V. CONCLUSION

We have confirmed the presence of O III Bowen fluorescence in UM 16, Akn 347, and III Zw 77, and reported its discovery in five other objects: Mrk 975, Mrk 359, MCG 8-11-11, Mrk 1388, and Mrk 1126. In addition to O III λ3133 (the strongest expected line), which all the sample objects possess, several objects show O III λ3444 (the second strongest line). We report the first evidence of O III λ3341 in a Seyfert nucleus, found in UM 16, Mrk 359, Mrk 1388, and III Zw 77. This line, a secondary Bowen cascade, is produced following the cascade that gives rise to O III λ3133. The relative strengths of the O III Bowen lines are compared with atomic physics calculations. Sometimes the agreement is good; in the cases of poor agreement, additional blended Bowen and non-Bowen lines may be responsible for some of the observed emission. Mrk 359 may have N III Bowen lines (as in X-ray binaries; see Paper I).

The derived O III Bowen yields ($y_{\rm HeO}$ values) indicate that He II Lyα opacities are sufficiently small ($\sim 10^4$) that escape of the pumping photons may be more likely than resonant trapping. Photoelectric destruction of Lyα by continuum absorbers (e.g., H I, He I) is probably unimportant in the radiative transfer.

Electron density diagnostics were derived from the [O III] line ratio $(I_{5007} + I_{4959})/I_{4363}$ and the [S II] line ratio I_{6716}/I_{6731}. For each of the galaxies in the *Rare Group* (UM 16, Akn 347, Mrk 1388, and Mrk 1126), we set a constraint on the Bowen emission-line region (ELR) density, typically $10^2 \lesssim n_e \lesssim 4 \times 10^4$ cm^{-3}. On the other hand, for the *Dense Group*, we were able to specify the Bowen ELR density more precisely (typically, $n_e = 4 \times 10^5$ cm^{-3}).

By using a published X-ray nebular calculation and the transfer physics of the Bowen process, we have constructed a model for the Bowen-emitting region. The model assumes a spherical volume of emission (radius $R_{\rm em}$) occupied by a number (N_c) of spherical clouds of size r_c; the clouds, each of density n_e, fill a portion (f_V) of the total volume. Using the forbidden-line density constraints, we solved for N_c and r_c and derived upper and lower limits for $R_{\rm em}$ and f_V (respectively). We find $R_{\rm em} \lesssim 1$–10 pc, $N_c \approx 10^9$–10^{13}, $r_c \approx$ 1–1000 AU, and $f_V \gtrsim 10^{-7}$ to 10^{-3}. The values of $R_{\rm em}$ and f_V are roughly consistent with previous NLR measurements. Also, the derived values of N_c and r_c are similar to those of well-studied BLRs. Typical covering factors are of order unity, so that the clouds cover the central source. The column density is low enough that these clouds are transparent to the soft X-ray continuum. The total cloud mass required is 100–10^6 $M_\odot$.

Our results suggest that observations of the Bowen process in other AGNs can be used to help understand NLR structure. Better studied AGNs may be used to test our simple model. Future X-ray data, revealing the shape of the underlying ionizing continuum, will complement our knowledge of Bowen fluorescence.

Note added in manuscript 1990 May 17.—Recently we received a preprint from Treves *et al.* (A. Treves, G. Bonelli, L. Chiappetti, R. Falomo, L. Maraschi, G. Tagliaferri, and E. G. Tanzi (*Ap. J.*, **359**, 98 [1990]) detailing new X-ray and *IUE* observations of MCG 8-11-11. The hydrogen column density inferred from their data is $N_{\rm H} \approx 1.0 \times 10^{21}$–$3.5 \times 10^{21}$ cm^{-2}. From Bohlin, Savage, and Drake (*Ap. J.*, **221**, 132 [1978]) we derive $E_{B-V} \approx 0.11$–0.90 mag, consistent with the reddening determination from our observations (Table 4).

This research was supported by grants from the California Space Institute, the Institute for Geophysics and Planetary Physics at Lawrence Livermore National Laboratory, the National Science Foundation, and the NASA Innovative Research Fund. We thank the referee, Tim Kallman, for insightful questions and useful criticisms. Also, we thank Anand Bhatia, Jules Halpern, Duane Liedahl, and Pat McCarthy for useful discussions, and Michael Strauss for making valuable comments on an earlier version of this paper. Help with the observations was provided by the day and night assistants at Lick Observatory, which is partly supported by NSF Core Block grant 86-14510 to the University of California.

REFERENCES

Bowen, I. S. 1934, *Pub. A.S.P.*, **46**, 146.
Cohen, R. D. 1983, *Ap. J.*, **273**, 489.
Davidson, K., and Kinman, T. D. 1978, *Ap. J.*, **225**, 776.
Deguchi, S. 1985, *Ap. J.*, **291**, 492; **303**, 901 (1986).
Eastman, R. G., and MacAlpine, G. M. 1985, *Ap. J.*, **299**, 785.
Eissner, W., and Seaton, M. J. 1974, *J. Phys. B*, **7**, 2533.
Ferland, G. J., and Netzer, H. 1983, *Ap. J.*, **264**, 105.
Ferland, G. J., and Osterborck, D. E. 1987, *Ap. J.*, **318**, 145.
Filippenko, A. V. 1982, *Pub. A.S.P.*, **94**, 715.
Filippenko, A. V., and Halpern, J. P. 1989, private communication.
Goodrich, R. W. 1989, *Ap. J.*, **324**, 224.
Halpern, J. P. 1982, Ph.D. thesis, Harvard University.
Halpern, J. P., and Steiner, J. E. 1983, *Ap. J. (Letters)*, **269**, L37.
Harrington, J. P. 1972, *Ap. J.*, **176**, 127.
Hummer, D. G., and Storey, P. J. 1987, *M.N.R.A.S.*, **224**, 801 (HS).
Kallman, T. R. 1989, private communication.
Kallman, T., and McCray, R. 1980, *Ap. J.*, **242**, 615 (KM80).
———. 1982, *Ap. J. Suppl.*, **50**, 263 (KM82).
Koski, A. T. 1978, *Ap. J.*, **223**, 56.
Malkan, M. A. 1986, *Ap. J.*, **310**, 679.
Miller, J. S., and Stone, R. P. S. 1987, *Lick Obs. Tech. Rept.*, No. 48.
Netzer, H., Elitzur, M., and Ferland, G. J. 1985, *Ap. J.*, **299**, 752.
Netzer, H., and Wills, B. J. 1983, *Ap. J.*, **275**, 445.
Osterbrock, D. E. 1981, *Ap. J.*, **246**, 696.
———. 1985, *Pub. A.S.P.*, **97**, 25.
———. 1989, *Astrophysics of Gaseous Nebulae and Active Galactic Nuclei* (2d ed.; Mill Valley: University Science Books), p. 338.
Osterbrock, D. E., and Mathews, W. G. 1986, *Ann. Rev. Astr. Ap.*, **24**, 171.
Osterbrock, D. E., and Pogge, R. W. 1985, *Ap. J.*, **297**, 166.
Peterson, B. M. 1988, *Pub. A.S.P.*, **100**, 18.
Petre, R., Mushotzky, R. F., Krolik, J. H., and Holt, S. S. 1984, *Ap. J.*, **280**, 499.
Phillips, M. M. 1978, *Ap. J. Suppl.*, **38**, 187.
Saraph, H. E., and Seaton, M. J. 1980, *M.N.R.A.S.*, **193**, 617 (SS).
Schachter, J., Filippenko, A. V., and Kahn, S. M. 1989, *Ap. J.*, **340**, 1049; erratum submitted (1990) (Paper I).
Seaton, M. J. 1979, *M.N.R.A.S.*, **187**, 73P.
Shuder, J. M., and Osterbrock, D. E. 1981, *Ap. J.*, **250**, 55.
Stasińska, G. 1984, *Astr. Ap. Suppl.*, **55**, 15.
Sternberg, A., Dalgarno, A., and Roueff, E. 1988, *Comm. Ap.*, **13**. 29.
Stirpe, G. M., de Bruyn, A. G., and van Groningen, E. 1988, *Astr. Ap.*, **200**, 9.
Véron-Cetty, M.-P., and Véron, P. 1987, *A Catalogue of Quasars and Active Nuclei* (3d ed.; Saint-Michel: Observatoire de Haute Provence), p. 102.
Yee, H. K. C. 1980, *Ap. J.*, **241**, 894.

ALEXEI V. FILIPPENKO: Department of Astronomy, University of California, Berkeley, CA 94720
[BITNET: alex@ucbbkyas.bitnet, INTERNET: alex@bkyast.berkeley.edu, SPAN: 42215::alex]

STEVEN M. KAHN: Department of Physics, University of California, Berkeley, CA 94720
[INTERNET: steve@xal.berkeley.edu]

JONATHAN SCHACHTER: Harvard-Smithsonian Center for Astrophysics, 60 Garden Street, Cambridge, MA 02138
[INTERNET: shaks@cfa.harvard.edu]